BOEING SCIENTIFIC RESEARCH LABORATORIES DOCUMENT D1-82-0586

BOEING

SCIENTIFIC RESEARCH LABORATORIES

AD 645548

Review of Lunar Infrared Observations

"Also available from the Author"

J. M. Saari

R. W. Shorthill

ARCHIVE COPY

DDC
RECEIVED
JAN 24 1967
C

GEO-ASTROPHYSICS LABORATORY DECEMBER 1966

D1-82-0586

REVIEW OF LUNAR INFRARED OBSERVATIONS*

by

J. M. Saari and R. W. Shorthill
Geo-Astrophysics Laboratory
Boeing Scientific Research Laboratory
Seattle, Washington 98124

December 1966

*Presented at the Symposium on "The Physics of the Moon," December 29, 1966 in connection with the 133rd Meeting of the American Association for the Advancement of Science, Sheraton Park Hotel, Washington, D. C.

ABSTRACT

Prior to 1960 the lunar surface was known to be highly insulating from the low temperatures observed during an eclipse and the lunar night. Directional effects in the infrared emission from the illuminated surface were understood to result from roughness. In 1960, a number of ray craters were shown to cool more slowly than their environs during an eclipse. Subsequently, this behavior was observed during the lunar night for both ray craters and certain other features. In 1964, the entire disk was scanned during a total eclipse, revealing the presence of hundreds of "hot spots." These anomalies have been identified with a variety of geological features. The current status of the thermophysical and geological interpretations of this discovery is discussed.

TABLE OF CONTENTS

	Page
LIST OF FIGURES	i
INTRODUCTION	1
MEASUREMENTS ON THE MOON BEFORE 1960	2
MEASUREMENTS ON THE MOON DURING 1960	3
DARKSIDE MEASUREMENTS	4
ILLUMINATED SURFACE MEASUREMENTS	7
ECLIPSE MEASUREMENTS	9
SURVEYOR I MEASUREMENTS	14
DISCUSSION	15
REFERENCES	41

LIST OF CAPTIONS

		Page
Fig. 1.	Eclipse cooling curve for a point 0.05 radius from the south limb of the moon, June 24, 1927, and for a point near the center of the disk, October 27, 1939.	19
Fig. 2.	Distribution of planetary heat across the disk of the full moon.	19
Fig. 3.	Isothermal contours of brightness temperatures for November 10, 1959 (start - 2:17, end 5:23 UT: 63 scans; 0.77 illuminated) (after Geoffrian et al., 1960).	20
Fig. 4.	Original data without Ge filter (0.5 to 15 microns) and with Ge filter (1.8 to 15 microns). Smoothed data from typical scans of Tycho during eclipse of March 12, 1960 at 0:53 PST.	20
Fig. 5.	Cooling curve for Tycho and its environs during the eclipse of September 5, 1960 (after Sinton, 1960).	21
Fig. 6.	Normalized cooling curves for Aristarchus, Copernicus, and Kepler for the eclipse of September 5, 1960.	21
Fig. 7.	Isothermal contours of brightness temperatures in the region of Aristarchus during the eclipse of September 5, 1960 at 10:12 UT.	22

Page

Fig. 8. Isothermal contours of brightness temperatures in the region of Copernicus during the full moon of September 5, 1960 at 5:48 UT. 22

Fig. 9. Equatorial brightness temperature versus days after local sunset. 23

Fig. 10. A typical lunar scan showing the derivative of the intensity profile at 20 microns (after Low, 1965). 23

Fig. 11. Infrared signal traces from the darkside measurements September 10, 1963 on the 22.3-day-old moon. 24

Fig. 12. Contour map of brightness temperatures on the nighttime portion of the third-quarter moon (after Wildey et al., 1966). 24

Fig. 13. Lunar nighttime traces through the crater Copernicus. 25

Fig. 14. Isothermal contours of brightness temperatures for the full moon. 26

Fig. 15. Isophotic contours of relative brightness for the full moon. 27

Fig. 16. Brightness temperature versus thermal longitude for phase angle -29°15'. 28

Page

Fig. 17. Brightness temperature versus observer's elevation angle to the surface with the sun at different elevation angles. 28

Fig. 18. Contours of the ratio of the brightness temperature on the thermal meridian to that of a Lambert surface as a function of the elevation angle of the sun and the angle of observation to the surface. 29

Fig. 19. Eclipse isothermal contours of brightness temperatures for the region of Tycho. 30

Fig. 20. Brightness temperature trace across Tycho during totality. 31

Fig. 21. Brightness temperature trace across the lunar disk north of the equator during totality. 32

Fig. 22. Isodensity contours of the number of hot spots per 10^5 km^2 lunar surface. 33

Fig. 23. Positions of 563 prominent hot spots on the lunar disk for the third scan in totality $3^H2^M.8$ UT, December 19, 1964. 34

Fig. 24. Distribution of thermal anomalies versus crater diameters. 35

Page

Fig. 25. Reconstructed infrared images of the totally eclipsed moon from 200 scan lines. 36

Fig. 26. Lunar Atlas Chart overlaid with isothermal contours of brightness temperatures from the totally eclipsed moon. 37

Fig. 27. The high-resolution oblique photograph of Copernicus taken from Lunar Orbiter II. 38

Fig. 28. Configuration of Surveyor I showing the position of the temperature sensor on Compartment A and B canisters. 39

Fig. 29. Lunation temperature curves for the lunar surface at the Surveyor I site. 39

Fig. 30. Brightness temperature ratios for the crater Tycho and its environs. 40

Fig. 31. Difference in energy ratios of the crater Aristarchus and interpolated environs during the eclipse of September 5, 1960. 40

REVIEW OF LUNAR INFRARED OBSERVATIONS

by

J. M. Saari and R. W. Shorthill

INTRODUCTION

The proximity of the moon to the earth has enabled astronomers to study its surface optically to a scale far finer than possible for any other object in the sky. While polarization and photometric measurements have indicated a fairly uniform surface layer, at least in terms of its texture, a wide variety of topographical features are evident on the surface, including craters of various ages, smooth maria, rills, domes, mountains, ray systems, dark halo craters, and rubble areas. Measurements in the electromagnetic spectrum outside of the optical region, prior to this decade, were confined because of instrumental or physical limitations to a small number of regions or to resolution elements comparable to the disk. Interpretations were limited therefore to global or typical properties of the surface, so that on this basis the microwave and infrared measurements yielded results consistent with the optical; thus the surface of the moon was generally understood to consist of

a highly insulating vesicular material which was sometimes colloquially, and sometimes seriously, described as dust.

In recent years, however, with the availability of more sensitive detectors, large antennas, and sophisticated computer techniques, it has been possible to explore the lunar surface at wavelengths outside the optical region to much finer detail than heretofore feasible. In two areas, where this has been pursued most successfully, that is the infrared and radar, an unexpected diversity of detail, comparable to that revealed by photographs, has been discovered. Comparison of these new results with geological data on the moon has sometimes resulted in a satisfying agreement with previous theories. On the other hand, certain of the new results reveal a number of features which seem to be characteristic of the wavelengths employed which have no optical, that is, topographical, counterpart. These measurements indicate that the moon has a highly diverse surface.

In this paper we review only briefly early thermal infrared measurements on the moon, concentrating for the most part on the results since 1960. We emphasize the experimental results with only a brief discussion of interpretation, inasmuch as the measurements have revealed a great amount of detail which is currently being compared to theoretical models and other experimental data such as high resolution photography.

MEASUREMENT ON THE MOON BEFORE 1960*

Although lunar infrared measurements were made as early as 1868, the definitive early work in the field was done by Pettit and Nicholson (1930) and Pettit (1940) at the Mount Wilson Observatory. In 1927 and 1939 measurements were made during lunar eclipses (Figure 1) when the surface was found to cool rapidly during the penumbral phase, the umbral temperature being about half that initially. Since finely divided powder or dust would behave in this way, it was proposed that the moon was

---

*Excellent reviews of this period have been written by Pettit (1961), Sinton (1962), and Zel'tser (1962).

covered with a dust-like material. In addition to the eclipse measurement, Pettit and Nicholson determined the general form of the temperature variation at full moon along the equator (Figure 2). If the lunar surface were perfectly diffuse (i.e., Lambertian) the temperature should vary as $\cos^{1/4}\theta$, where θ is the angular distance from the subsolar point. They found, however, that the variation was more like $\cos^{1/6}\theta$, attributing the difference to a general roughness of the surface. During the lunar night, they observed the surface to cool even more than during an eclipse, reporting a temperature of 120°K for the anti-solar point.

An important series of infrared measurements were made during the 1950's at the Lowell Observatory by W. M. Sinton. In addition to repeating the previous eclipse measurements, he and his co-workers made thermal maps of the illuminated surface through a lunation for nine different phase angles. The moon was scanned with a television-like raster using the earth's rotational motion and the moon's motion in declination (Geoffrion et al., 1960). The resolution was about $1/72$ of a lunar diameter (Figure 3). Because of this limited resolution, correlations with surface features were difficult; however, Mare Crisium was observed to be somewhat warmer than its environs (uplands).

MEASUREMENTS ON THE MOON DURING 1960

During the March 13, 1960 lunar eclipse a group from The Boeing Company, using the 72-inch telescope of the Dominion Astrophysical Observatory, planned to obtain cooling curves on a variety of lunar features; the idea was to determine whether the surface cooled uniformly or not. Because of poor weather conditions, this plan was abandoned. However, it was possible to scan the detector across the lunar surface during totality, when it was discovered that the ray crater Tycho (Figure 4) remained warmer than its environs. Although many other craters in the same region did not show this anomalous behavior, there was evidence that Aristarchus and Copernicus also cooled more slowly (Shorthill et al., 1960).

Another eclipse in September 1960 provided an opportunity to verify and extend these surprising results. At the Lowell Observatory, Sinton

(1960), using a Golay cell in the 7.3 to 10.3 micron band, obtained a cooling curve for Tycho and its environs (Figure 5). During the same eclipse cooling curves for Aristarchus, Kepler, and Copernicus (Figure 6) were obtained with a thermistor bolometer in the 8 to 14 micron band on the Mount Wilson 60-inch telescope (Saari and Shorthill, 1963). In addition, maps were made of the regions of these craters and Tycho and Proclus as well during totality at a resolution of $1/250$ of the lunar diameter. The thermal map of Aristarchus (Figure 7) shows that the anomalous region is (1) maximum at the crater center, (2) extends beyond the crater rim, and (3) falls to the environ value about a crater diameter from the rim. This was also found to be true for Tycho and Kepler. The anomalies were interpreted in terms of a "dust" layer thinner than its environs, Sinton proposing that the temperature difference could be used to date the age of the craters.

On the full moon before and after this eclipse, we made scans on eleven different crater regions which were correlated with specific features. The structure observed in these thermal maps on the illuminated moon seemed attributable to local differences in albedo and/or inclination of the surface (geometry). The effect of albedo is seen in Figure 8 where the contours going around Copernicus bulge to the left outlining the bright debris blanket. The effect of geometry is demonstrated by the fact that the western interior slopes are warmer than the eastern interior slopes because they are more directly illuminated by the sun.

DARKSIDE MEASUREMENTS

In recent years, the sensitivity and speed of infrared detectors have been improved markedly over the thermocouples, thermistors, and the Golay cells used previously. Murray and Wildey (1964), using a mercury-doped germanium photodetector, were able to make measurements on the darkside of the lunar surface where the temperatures are much lower than found during an eclipse. Their technique was to position the detector on an illuminated feature near the sunset terminator, scan the telescope in right ascension onto the darkened portion of the disk and off the limb into the sky, reverse, and scan back in the opposite direction,

stopping again on the illuminated surface. The moon's motion in declination generally displaced the two scans slightly. One example of their results for a scan near the equatorial region is shown in Figure 9, along with similar results obtained by the authors using the same type of detector and scanning technique. The data are plotted in terms of days beyond local sunset (rather than position) to reveal the cooling characteristics of the general surface. There are some differences between the two curves, possibly caused by drifts in sky background. By extrapolation of the curves, it appears the value for the midnight temperature reported by Pettit and Nicholson (1930) of 120°K, and that by Sinton (1959) of 122°K is too high. A value ~100°K (Saari, 1964) may be more correct.

The unilluminated surface continues to cool for seven more days after midnight and therefore is coldest just before the dawn. Neither Murray and Wildey or the authors were able to detect the pre-dawn temperature, presumably because of variations in the sky background radiation. Frank Low (1965), however, working in the 17.5 to 22 micron window with his germanium bolometer and cancelling the sky background using a differential technique, has been able to measure very low temperatures. Figure 10 shows a typical scan of the derivative of the intensity profile over the darkened disk. The off-scale deflections occur at the hot limb and terminator. The smaller positive deflection at the right represents the cold limb. He found a mean temperature of 90°K for the darkened disk; the coldest temperature observed was ≤70°K.

Measurements on the unilluminated portions of the third-quarter moon have been made by Shorthill and Saari (1965*a*); the individual traces are shown in Figure 11. The effect of drifts in the sky emission may be seen in that the "A" scans (moving west in right ascension) are in some cases shifted in temperature somewhat from the "B" scans (moving back east in right ascension). Scan 1B shows a temperature rise of 20° to 25°K reported originally as De La Rue but now known to be the ray crater Thales. Scan 3 shows a hot spot now identified as the crater Dawes. These data, as well as scans on other nights, indicated that not all hot

spots are associated with the bright ray craters as was the case during the 1960 eclipses.

Murray and Wildey (1964) have also reported several hot spots not associated with ray craters. By scanning the moon with 18 pairs of traverses requiring a period of several hours, Wildey, Murray, and Westphal (1966) were able to produce a detailed map of the unilluminated eastern hemisphere of the moon (Figure 12). The terminator shown in the heavy dashed line has an average temperature of 145°K, agreeing quite well with our results on the illuminated moon. Mare Crisium was observed to have a $\Delta T = 5°K$ above its environs. Many hot spots can be associated with craters; some are ray craters such as Menelaus and Dionysius, others such as Dawes, at 134.1°K with a $\Delta T = 6.6°K$, are not ray craters. Mare Tranquillitatis has a concentration of hot spots. Several of the anomalies are associated with features smaller than the resolution of the detector so that the indicated brightness temperatures may be too low.

Low (1965) has reported large variations above and below the mean temperature of 90°K observed on the darkside. In fact, one such hot spot (Figure 10) near the southern limb was found to have a temperature greater than 150°K with a $\Delta T > 60°K$. Low was not able to identify this feature; however, subsequent eclipse measurements by us indicate that it may be a hot spot in the region of Schomberger F or perhaps Tycho.

The crater Copernicus was scanned by Murray and Westphal (1965) and by the authors on the darkside. Figure 13 shows single scans through the crater from both sets of data. The surprising thing about these results is that the thermal structure is "washed out" and shows a Gaussian-like shape with a maximum within the crater; there is no evidence of a thermal pattern corresponding to the portions of the crater illuminated just before sunset. On the other hand, Salisbury and Hunt (1966) have recently made infrared images of Tycho after sunset which do reveal such a pattern.

ILLUMINATED SURFACE MEASUREMENTS

The isothermal maps of the illuminated disk made by Sinton and his co-workers were difficult to correlate with surface features. In 1962 a program of lunar measurements was begun at Boeing Scientific Research Laboratories to scan the illuminated disk through a lunation in both the far infrared and visible regions to a resolution of 8" arc ($1/240$th the lunar diameter). The purpose of this mapping project was to (1) determine whether there were infrared anomalies on the illuminated surface, (2) provide photoelectric data over the disk for a better determination of photometric function, (3) investigate the directional properties of the infrared emission, and (4) determine the detailed relationship between albedo and temperature. Data were obtained for 23 phases from -125° to +135° phase angle more or less uniformly spaced. The instrumentation, using a mercury-doped germanium photodetector for the infrared, has been described (Shorthill and Saari, 1965*a*; Saari and Shorthill, 1966). The contour maps, of which figures 14 and 15 for the full moon are examples, will be published in 1967 as a NASA publication.

Since the data have been only recently reduced and are presently in the process of being analyzed, we report here only several examples of the results obtained so far. Inspection of the contours shows that anomalies on the illuminated surface are rare occurrences; so far, only two areas are suspect, one east of Tobias Mayer A on the south shore of Mare Imbrium and the other south of Theophilus at about 18° latitude. Both areas appear cooler than their environs under illumination, although their albedo is not particularly greater. Otherwise the deviations in the infrared contours seem accountable for reasons of local changes in albedo or slope.

Perhaps the most anomalous behavior of the illuminated surface is the directionality of its infrared emission. The data have been studied in this respect (Montgomery, Saari, Shorthill, and Six, 1966) with reference to a set of thermal coordinates for 19 of the different phases. In this system, the subsolar point is the thermal pole (90° thermal latitude) and the terminator the thermal equator (0° thermal latitude). The thermal meridian (0° longitude) is the great circle through the subsolar

point and the topocentric disk center; thermal longitudes are measured from this meridian, being positive in a counterclockwise direction around the subsolar point. As an example, the data for phase angle -29° are shown in Figure 16; brightness temperatures were taken every 10° in thermal latitude and longitude. At high thermal latitudes (near the subsolar point), the brightness temperature is relatively constant. At lower latitudes, the curves are concave upward.

A particular study has been made of the brightness temperature along the thermal meridian. Measurements were made along the thermal meridian of each phase for elevation angles of the sun equal to 10°, 20°, 30°, ... 80°. Corrections were made for variations of the sun-moon distance and for variations of the local albedo at each point measured. Further, for each point the elevation angle of observation with respect to the surface was calculated. By plotting the brightness temperature at each sun angle as a function of elevation angle of observation, one obtains the curves shown in Figure 17 (each is a least-square polynomial fit to the measured points). In terms of an observer on the surface, the 90° observer elevation angle corresponds to his looking vertically down at the surface, 0° elevation to his looking at the horizon with the sun on his back, and the 180° elevation angle to his looking at the horizon facing the sun. The data having been taken along the thermal meridian, means in all cases the line of sight is in the plane defined by the rays and the normal to the surface element being observed. The curves reveal that for the low sun elevation angles of 10°, 20°, and 30° the highest brightness temperature is obtained for an observer elevation angle of 0°, i.e., the horizon. At higher sun elevation angles, the highest brightness temperature is obtained at an elevation angle somewhat lower than that of the sun.

These data have also been plotted in terms of a directional factor, defined as the ratio of the observed brightness temperature to the temperature of a Lambert (diffuse) surface radiating the same energy. In Figure 18 directional factors (D-factors) calculated for the thermal meridian data are shown as contours plotted as a function of the sun and observer elevation angles. In this plot, Sinton's data on the subsolar-

point variation with phase is the upper boundary of the figure; the lower boundary is the terminator. The horizon (i.e., the limb) looking into the sun is on the right and the horizon looking with the sun is on the left. In this figure, data for a particular phase angle g are found on lines inclined upward 45° from the horizontal; for instance, the D-factors along a line from the origin to the midpoint of the upper boundary are for the full moon. Likewise, D-factors along a line from the midpoint of the lower boundary to the upper right-hand corner are for the quarter moon ($g = \pm 90°$). For both cases, the D-factor is relatively constant near the subsolar point, but increases near the terminator.

Studies are continuing to determine the D-factors for all values of azimuth and elevation angles for the observer at several sun angles. Such data can be used to determine what geometrical configurations of the lunar surface can explain the observed directional characteristics of the infrared emission, and to calculate the heat balance of spacecraft on the surface.

ECLIPSE MEASUREMENTS

It had become increasingly evident that a detailed mapping of the entire unilluminated lunar disk would be necessary to determine just how many thermally anomalous regions exist. Measurements during eclipses had shown that ray craters cool less rapidly than their environs. Darkside measurements further revealed that other types of features were also hot spots. If such a mapping were done on the darkside, observations over many nights would be required, as well as slow scanning for accurate measurements of the low temperatures. During an eclipse, however, the temperatures are considerably higher and so a rapid-scan system could be used. We planned to so scan the disk using the Mount Wilson 60-inch telescope during the eclipse of December 30, 1963, but failed bacause of a high haze condition.

Arrangements were made a year later to use the 74-inch Kottamia telescope of the Helwan Observatory in Egypt for the eclipse of December 19, 1965. The rapid scanner was modified so that the entire disk could be covered by 200 traverses in 17 minutes with a resolution of $1/200$ of a

lunar diameter. On the basis of previous darkside and eclipse measurements, we expected to find that the major ray craters and possibly a few non-ray craters were hot spots. In addition to the ray craters already known to be hot spots, such as Aristarchus and Tycho, all the major ray craters such as Aristoteles, Dionysius, Langrenus, Menelaus, and Stevinus were indeed observed to be anomalous. An example of the eclipse isotherms for Tycho and its environs are shown in Figure 19. The peak temperature in Tycho was found to be 227.1°K or about 60°K warmer than its environs; a single traverse through Tycho is shown in Figure 20. In addition to the ray craters, we were astonished to see on most traverses many other "spikes" as the scanner moved across the lunar disk (Figure 21). These localized thermal anomalies number about 1000 and represent a most significant result concerning the thermal properties of the lunar surface (Saari and Shorthill, 1965*b*). Identifications have been made on several hundred hot spots for the purpose of studying the relationships to the visible surface features. It was quickly established that the majority of hot spots are visually bright in some way at full moon. Table 1 shows a preliminary classification based on 330 hot spots.

Table 1

PRELIMINARY CLASSIFICATION OF THERMAL ANOMALIES ON THE ECLIPSED MOON

Ray craters	19.4%	84.5%
Craters with bright interior at full moon	41.8%	
Craters with bright rims at full moon	23.3%	
Craters not bright at full moon	0.6	
Bright areas with much smaller crater	3.6	8.7%
Bright areas associated with features like ridges	3.9	
Bright areas not associated with any feature	1.2	
Position unidentified or questionable	6.3	

Approximately two-thirds of the hot spots fall in the seas and one-third in the highlands (Shorthill and Saari, 1965*b*). The statistical distribution of the 563 most significant hot spots over the hemisphere has been plotted in Figure 22. Several regions of high concentration are found; the greatest concentrations were found in Mare Tranquillitatis

($8/10^5$ km^2) and in a region between Kepler and Aristarchus ($6/10^5$ km^2). Using several different tests for randomness, it was determined that the concentration in Mare Tranquillitatis occurring by chance alone was less than one in 5000.

The 563 hot spots used in the previous figure are plotted on the lunar disk in Figure 23. In addition to the correlation with bright young craters, some of the hot spots have been identified with "white area," which may encompass very small craters: Linné, Posidonius γ, and the white region (near Hell Q and QA) in Deslandres are examples. Another class of features which exhibit anomalous thermal behavior are the maria. Mare Humorum, Mare Fecunditatus and Mare Tranquillitatis were found to be elevated above their environs while only parts of Mare Frigoris, Mare Imbrium, and Oceanus Procellarum were elevated in temperature (Figures 20 and 21).

For the purpose of presenting a meaningful ordering of the thermal anomalies, 83 features giving the largest signal difference over their surroundings were studied. Many of these were associated with craters smaller than the resolution of the detector ($1/200$ lunar diameter) resulting in the observed temperature being too low. It was necessary to make an areal correction to the signal difference; for simplicity it was assumed that the anomaly originated only from the crater where radiance was uniform. The correction took into account the crater diameter, its projection onto the detector aperture, and the relative signal difference above the environs on successive traverses (occasionally the signal was observed on only one traverse). For the large craters like Tycho a value averaged over the crater was used. Of the 30 most prominent areally corrected craters ranked (Table 2), 6 are ray craters, 20 are craters with bright interiors and 4 have bright rims. Also, 23 fall in the maria and 5 in the uplands.

Table 2

RANKING OF 30 PROMINENT ANOMALIES ON THE ECLIPSED MOON

	Crater	Diameter (km)		Crater	Diameter (km)
1.	Mösting C	3.8	16.	Egede A	12.5
2.	Piton B	4.8	17.	Laplace A	9.7
3.	Messier A	13.6	18.	Nicollet	15.2
4.	Buch B	6.7	19.	Mösting A	13.0
5.	Jansen E	7.0	20.	Mason C	12.3
6.	Torricelli B	6.9	21.	Cauchy	12.3
7.	Draper C	7.7	22.	Gambart C	12.2
8.	Maraldi B	7.4	23.	Carlini D	9.3
9.	Moltke	6.4	24.	Eudoxus A	14.1
10.	Plato M	8.3	25.	Pico B	11.4
11.	Guericke C	10.9	26.	Cephus A	12.5
12.	Flamsteed B	9.4	27.	Hesiodus B	10.2
13.	Taruntius H	8.3	28.	Janssen K	15.5
14.	Jansen F	9.4	29.	Bode A	12.3
15.	Marius A	16.0	30.	Carlini	11.4

A plot of crater diameter versus the areally corrected signal difference is shown in Figure 24 and represents about 6 percent of the hot spots detected at our resolution (Shorthill and Saari, 1965*c*). The larger signal differences are observed on the smaller craters. In fact most of these areally corrected hot spots (68 percent) are smaller than the sensor resolution. The data in Figure 24 represent the boundary of a general distribution for a large number of hot spots. It may reasonably be expected that as the resolution of the detector is improved a proportional increase in the number of hot spots will be observed. There is, however, an upper limit imposed on the signal difference over the environs assuming that the value of the thermal parameter γ is not less than 20 (bare rock). For example, Mösting C was observed to have a $\Delta T = 28°K$ above its environs while its areally corrected difference was $\Delta T_c \approx 157°K$: other examples are Messier A with $\Delta T = 42°K$ and $\Delta T_c \approx 113°K$; Gambart C with $\Delta T = 32°K$ and $\Delta T_c \approx 41°K$; Torricelli B with $\Delta T = 26°K$ and $\Delta T_c \approx 90°K$. Location of these hot spots on the plot in Figure 24 can be found by

counting down from the highest point in the ranking.

Since the data were recorded on magnetic tape it was possible to construct images of the infrared data (10 to 12 microns). The signal was used to modulate the intensity of an oscilloscope while the scan raster was reproduced. A photograph of the face of the oscilloscope is shown in Figure 25 for the totally eclipsed moon of December 19, 1964. The 17 most prominent areally corrected hot spots are indicated along with other features including several of the large ray craters. The large areas of thermal enhancements previously discussed are easily observed on the image (e.g., Mare Humorum). Traverse number 31 (Figure 20) can be identified by finding Heinsius A just to the left of Tycho. The bright region in the lower right of the image is caused by radiation from the side of the telescope. During the eclipse measurements three complete disk scans were made during totality, four during the penumbral phase and several on the full moon. Images of all these data have been published (Saari, Shorthill and Deaton, 1966).

The isothermal contour map for the last scan in totality has been transferred to a Mercator projection for ±70° longitude and ±16° latitude. These projections have been constructed at a scale suitable for overlaying onto the LAC* Quadrangles. The projections can also be overlaid onto the Geologic Maps† produced by the U. S. Geological Survey for the purpose of studying the relationship to the thermal data. A portion of the Copernicus Quadrangle (LAC 58) is shown in Figure 26 overlaid with the projections of the isothermal contours. The dashed lines show the approximate field of view of the moderate resolution oblique photograph taken from Lunar Orbiter II of the Copernicus region,

---

*Lunar Atlas Chart Quadrangles have been published by the U. S. Air Force Aeronautical Chart and Information Center, St. Louis, Missouri, 63118. The charts are 20° longitude by 16° latitude at a 1,000,000:1 scale.

†These maps show the geological classifications of lunar features and use the LAC Quadrangles as a base.

November 24, 1966 at 00^H5^M UT. Copernicus H, a dark halo crater with a sharp rim 30 km southeast of Copernicus, is a hot spot with a $\Delta T = 22°K$. This can be seen on the moderate resolution frame two-thirds of the way to the edge of the frame and two framelets down from Copernicus. A portion of the high resolution photograph is shown in Figure 27 with several eclipse brightness temperatures indicated. The temperature values are not readings at a point but rather for the general region of the crater floors, peaks, rims, etc. The primary photographic sites for Lunar Orbiter I and II were chosen mostly in relatively flat regions in support of the Apollo landing-site selection. For this reason hot spots as such were not included because they are in general associated with bright young features that are likely to be rough and have debris strewn environs therefore not yet appropriate for landing sites. In fact, the Surveyor I and II sites avoided rough areas (i.e., hot spots) for the same reason. In the case of Lunar Orbiter, several secondary photographic sites did cover regions known to be hot spots. Dionysius was photographed on Lunar Orbiter I on moderate resolution frame number 84, revealing large rocks or boulders ($\sim$30 meters) on the outside slopes of the crater. The resolution, however, was not sufficient to determine if the surface roughness is a significant factor in the explanation of the hot spots. Frame number 31 covers the Taruntius region where Taruntius K,P,H and an unamed crater are hot spots. The resolution again was a limiting factor in observing a significant departure from other features which do not exhibit anomalous thermal behavior. Several of the high resolution frames from Lunar Or r II show some rock-strewn fields in Mare Tranquillitatis and some extremely rough crater interiors. Here the photographic resolution is sufficient but the areas are too small to show up in our eclipsed data.

SURVEYOR I MEASUREMENTS

The successful landing of Surveyor I on the moon on June 2, 1966 provided an opportunity to make *in situ* measurements of lunar infrared emission (Jaffe et al., 1966). Although the spacecraft was designed to be thermally insensitive to its environment, there were two insulated electronic compartments (designated A and B) or which the temperatures

of the outboard faces were monitored after touchdown. Compartment B was oriented so that the normal to the outboard face was pointing approximately 30° west of north and 20° above the horizon (Figure 28). The temperature of this face was determined by the balance of the energy radiated to the energy received from the sun and from the lunar surface (both the reflected light and the infrared). With knowledge of the emissivi and absorptivity of the compartment surface and its temperature, it was then possible to calculate a value of the lunar surface temperature. Measurements were made during the first lunar day the spacecraft was on the surface and for 48 hours after sunset; the resulting calculated lunar surface temperatures are shown in Figure 29 (the nighttime values include a correction for a certain amount of heat leakage from the interior). A comparison with Lambert temperatures calculated taking into account the sun-moon distance and the local albedo determined from earth-based measurements shows agreement near local noon. The values during the night correspond to a homogeneous surface with a thermal parameter $\gamma \sim 1000$, which agrees reasonably well with a value of ~ 1300 determined from eclipse observations of the area (to a resolution of ~ 20 km).

Before noon the inferred values from Surveyor I are higher than the predicted Lambert temperatures. This is not surprising in view of the directional characteristics of lunar emission as discussed in Section V. For a comparison, data from our earth-based observations of the area through a lunation are also shown in the figure. Because of the location of the landing point, our detector observed the area at an elevation angle of 45° from east. The same general shape in the curve is observed as from Surveyor. Currently work is underway to determine whether the directional characteristics observed globally from earth-based measurements can satisfactorily account in detail for the daytime measurements from Surveyor. If so, this would indicate these directional characteristics are operative on a scale of dimensions comparable to that of the Surveyor scene.

DISCUSSION

The recent measurements on the illuminated disk with phase have shown

the dominating influence of the solar radiation in determining the observed brightness temperatures. Local differences in temperature are caused by variations in slope and albedo. The most noticeable effect observed on the illuminated surface is the directionality of the emission, which qualitatively can be understood in terms of surface roughness. Further work in this area could include data reduction in determining the directional factor in all directions from an element of illuminated surface and calculations on geometrical models of surface roughness for fitting to the experimental data. For instance, Hapke (1966) has recently proposed a wrinkled model of the surface to improve the fit of his theoretical photometric function to observations near the limb. It would be interesting to see if the same model of roughness can account for both the photometric and the infrared data. Directional effects were also apparently observed from temperature measurements made from the Surveyor I spacecraft, which in general were compatible with earth-based measurements for the same area.

It is during the absence of sunlight, either during an eclipse or during the lunar night, that the thermophysical properties of the surface are most strikingly revealed. It is now known that the lunar surface possesses extensive thermal heterogeneity, the thermal features observed characteristically maintaining a higher temperature than their environs during cooling. The interpretation of these data would ideally involve the comparison of cooling curves with theoretical models. Since the cooling curves from our own eclipse data are in the process of being reduced, no results can be reported at this time. However, work by Ingrao, Young, and Linsky (1966) may serve as an illustration of the possible ultimate limitations of this approach. They made infrared measurements during the eclipse of December 19, 1964, and in particular, obtained cooling curves for the crater Tycho. They then considered a variety of theoretical models to account for its anomalous cooling compared to its environs and to compare with darkside measurements. The models investigated included the homogeneous model with temperature-independent thermal parameters, a two-layer model, and a homogeneous model in which the thermal conductivity and heat capacity were linear

functions of temperature, and a homogeneous model in which the thermal conductivity had a constant term plus a radiative term proportional to T^3. Their conclusion was that the Tycho data were best fit by a two-layer model (Figure 30), whereas the lunation data were better represented by the latter two homogeneous models. However, the differences between the various models was not so great that a definitive choice could be made. Winter (1966*a*) has considered a pure radiation model consisting of parallel flat slabs and was able to obtain agreement with our eclipse data for Copernicus with slabs 0.05 cm thick compared to a thickness of 0.015 cm for its environs. For a lunation, the latter was calculated to have a midnight temperature somewhat below 100°K.

The above models assume horizontal homogeneity of the surface. If this restriction is relaxed other explanations are possible in accounting for the thermal anomalies. Bastin (1965) suggested that a rough surface would appear to an infrared detector to cool more slowly, the idea being that the declivities in the surface could not lose their heat as rapidly because their view of cold space is restricted. Winter (1966*b*) showed that a surface, 10 percent of which was covered with declivities on a centimeter or greater scale, could account for the anomalous eclipse cooling of Aristarchus (Figure 31). Also, the presence of a large number of rocks on the surface could cause a slower cooling; Sinton (1960) calculated his observations on Tycho could be accounted for by 11 percent of the surface being covered by rock. Since that time the Surveyor I has convincingly demonstrated that rocks do exist on the surface, so that some of the hot spots, particularly the ray craters, may be rubble areas where bare rocks and enhanced roughness may both contribute to their being anomalous. Recently, the photographs from the Lunar Orbiters I and II have further confirmed the presence of rocks on the surface. For instance, fields of rock were found in the southwestern portion of Mare Tranquillitatis, the region on the moon having the highest concentration of hot spots. This suggests that high resolution photographs of the lunar surface may prove decisive in the interpretation of the infrared results.

Theoretical calculations are needed on the response of rocks of different sizes to eclipse and lunation cooling, since the effects may be expected to be different in the two cases because of the different time scales involved. There is evidence that the thermal pattern on anomalies is different during eclipse and lunation cooling. In the case of Copernicus, during an eclipse three maxima in the brightness temperature were observed within the crater, whereas with the same resolution, only one maximum was seen 16 hours after sunset. Thus a careful comparison of darkside and eclipse infrared mapping may show differences which, in the case of the rock hypothesis, could be due to variations in the size distribution.

Thermal anomalies have been identified with a number of different kinds of geological features such as ray craters, bright-rimmed craters, white areas, and rills; in some cases it has not been possible to identify a feature for the hot spot. Because of the diversity of the features identified with anomalies, it would not be surprising if they arise because of an equally diverse number of geological reasons. Fudali (1966) has suggested that slumping on the steep interior slopes of craters has kept fresh material exposed on these surfaces, accounting for both their high albedo and anomalous thermal behavior. The photographs from Lunar Orbiter II indeed show steep slopes with evidence of slumping on the interior rims of Copernicus and its central peaks. Thermally, certain ray craters show a maximum response from the interior rims, of which Langrenus is an example. Also, certain of the older craters like Reinhold, having only a mild infrared enhancement over their environs, often have a maximum response on the interior rim. They may represent craters in the final stages of their "thermal" evolution. Other geological processes may have been operative in producing the conditions for anomalies; the so-called white areas such as Posidonius γ may have been formed by the deposition of a sublimate, locally increasing the thermal conductivity or density (Shorthill and Saari, 1965*c*). Thus the infrared cooling data may represent an important source of geological information to aid in the planning of future exploration of the moon.

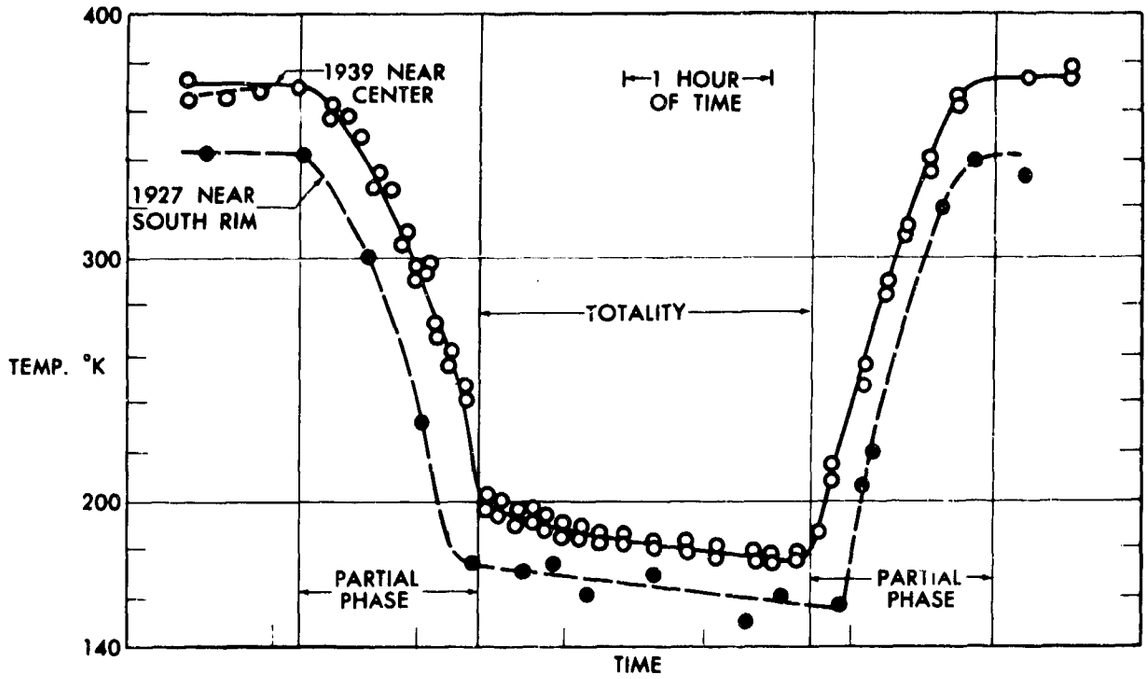

Fig. 1 Eclipse cooling curve for a point 0.05 radius from the south limb of the moon, June 24, 1927, and for a point near the center of the disk, October 27, 1939.

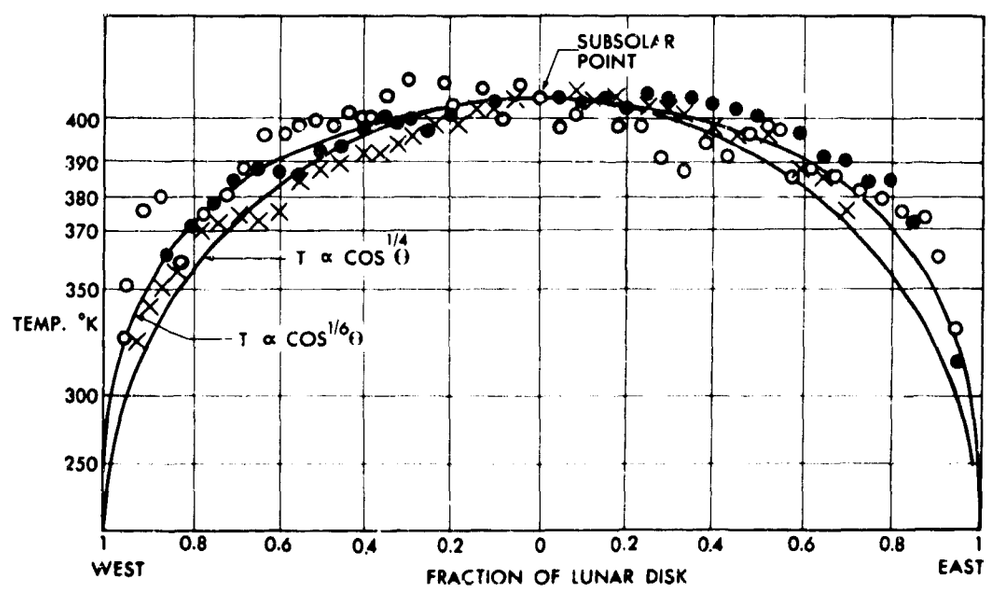

Fig. 2 Distribution of planetary heat across the disk of the full moon. The various symbols represent different sets of measurements.

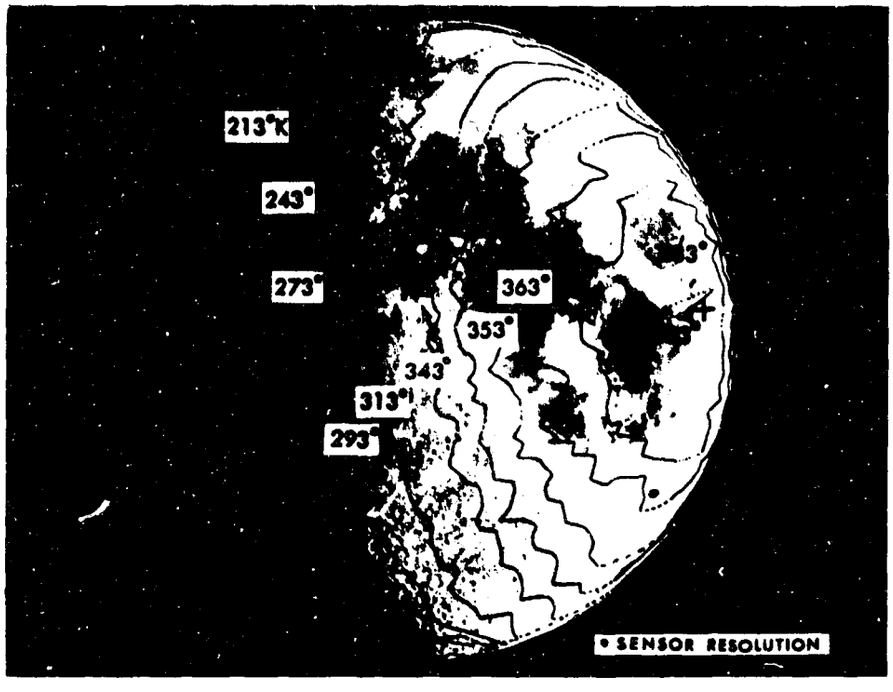

Fig. 3 Isothermal contours of brightness temperatures for November 10, 1959 (start - 2:17, end - 5:23 UT: 63 scans; 0.77 illuminated) (after Geoffrian et al., 1960).

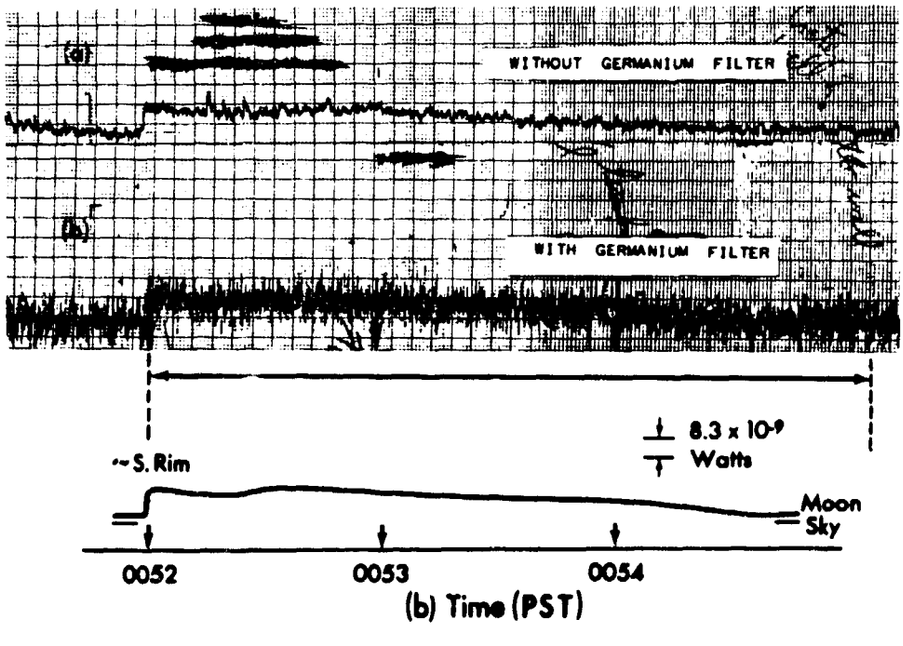

Fig. 4 Original data (a) without Ge filter (0.5 to 15 microns) and (b) with Ge filter (1.8 to 15 microns). Smoothed data from typical scans of Tycho during eclipse of March 12, 1960 at 0:53 PST.

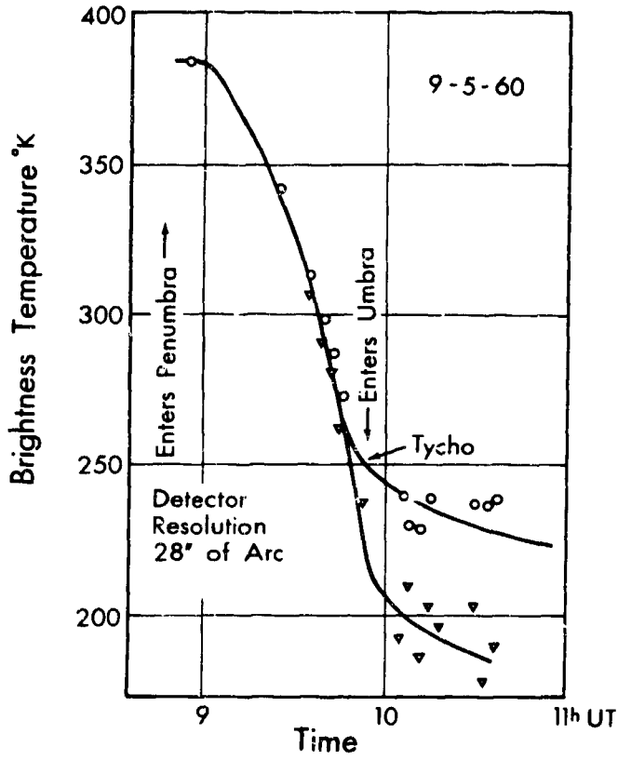

Fig. 5 Cooling curve for Tycho (circles) and its environs (triangles) during the eclipse of September 5, 1960 (after Sinton, 1960).

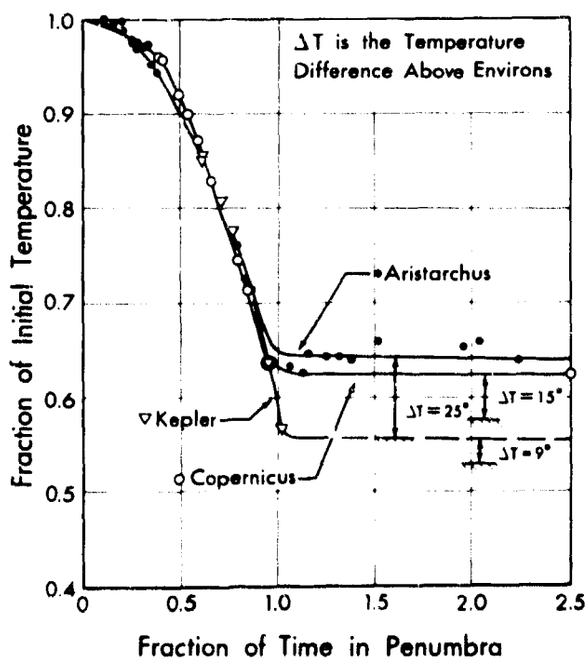

Fig. 6 Normalized cooling curves for Aristarchus, Copernicus, and Kepler for the eclipse of September 5, 1960. The ΔT refers to the temperature difference above the environs.

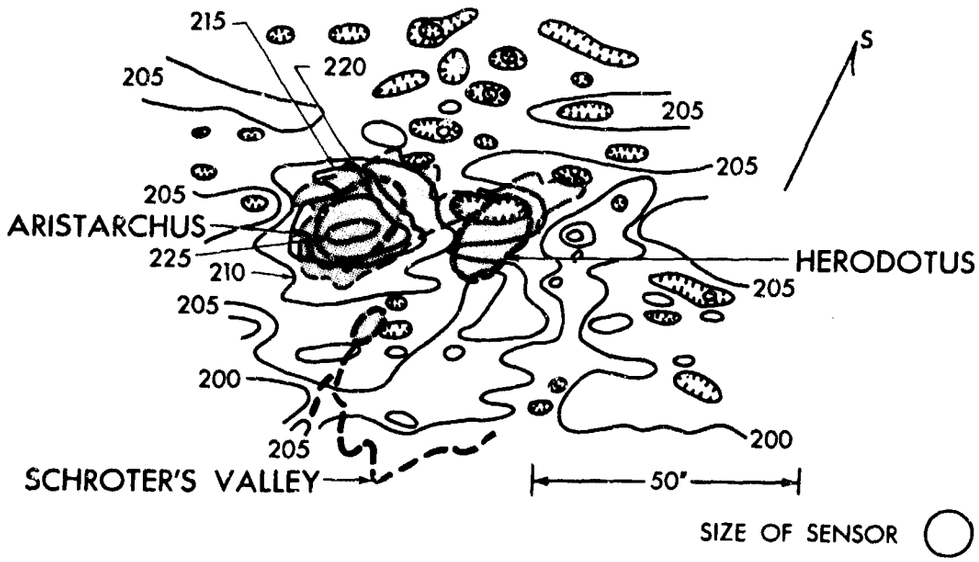

Fig. 7 Isothermal contours of brightness temperatures in the region of Aristarchus during the eclipse of September 5, 1960 at 10:12 UT. The shaded area outlines the region of high albedo.

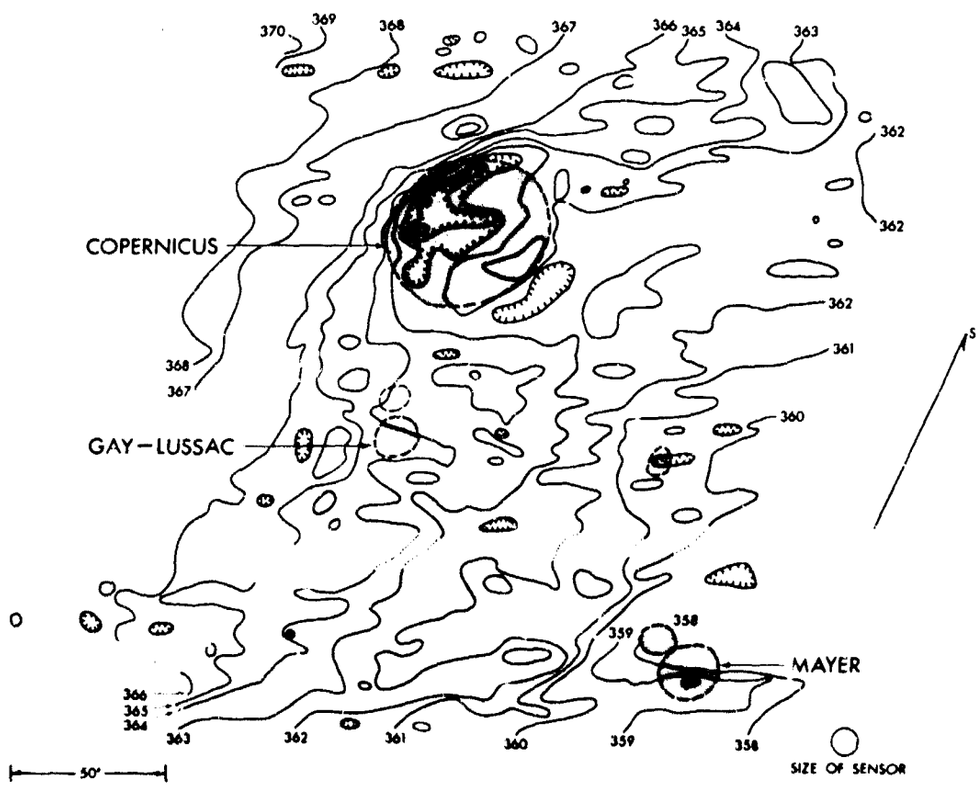

Fig. 8 Isothermal contours of brightness temperatures in the region of Copernicus during the full moon of September 5, 1960 at 5:48 UT.

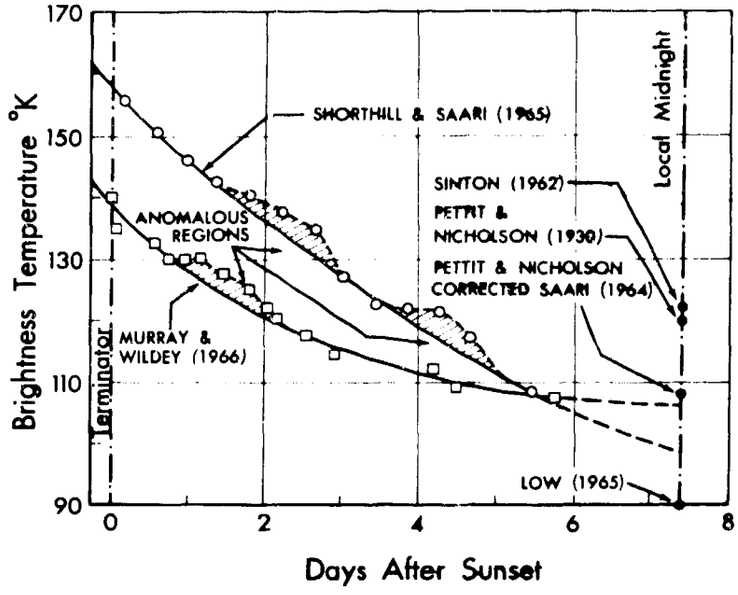

Fig. 9 Equatorial brightness temperature versus days after local sunset. The data were extrapolated to give a midnight temperature. Other measurements of the midnight temperature are indicated.

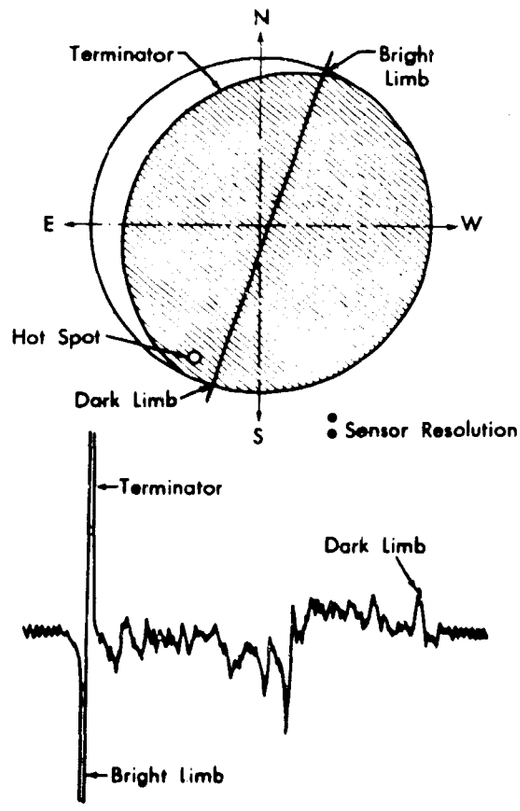

Fig. 10 A typical lunar scan showing the derivative of the intensity profile at 20 microns (after Low, 1965). The hot spot has been tentatively located in the region of Schomberger F using the eclipse data of Saari and Shorthill.

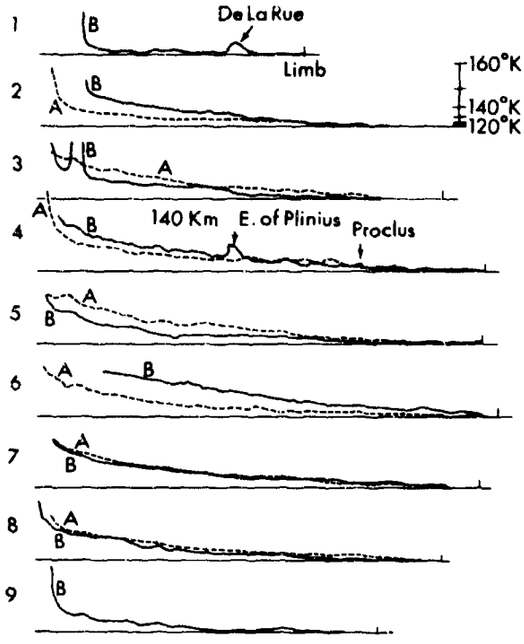

Fig. 11 Infrared signal traces from the darkside measurements September 10, 1963 on the 22.3-day-old moon. The off-scale deflection on Scan 3B results from a protruding feature beyond the terminator still illuminated by the setting sun.

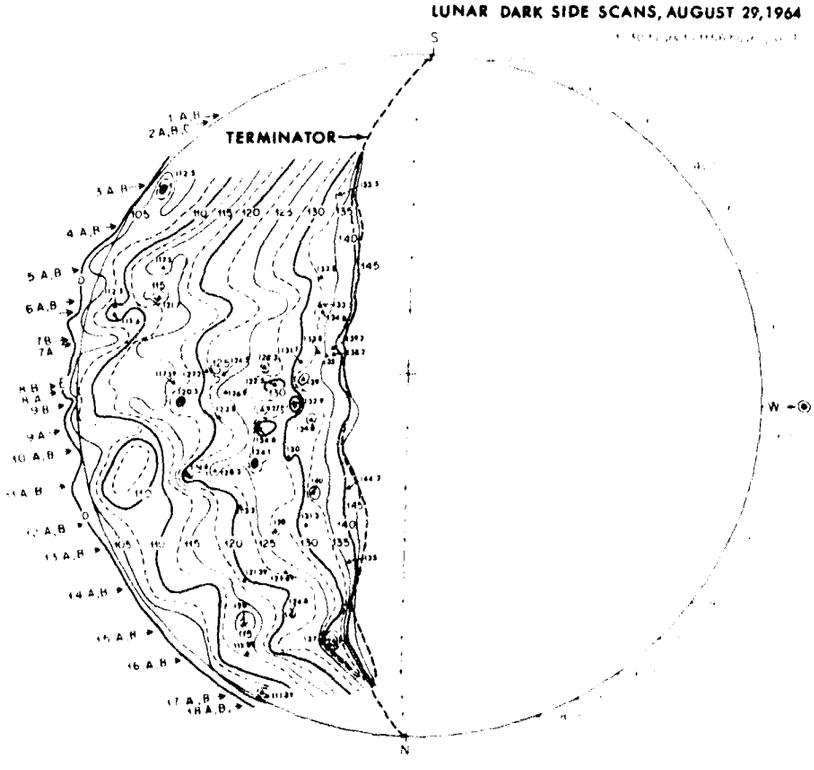

Fig. 12 Contour map of brightness temperatures on the nighttime portion of the third-quarter moon (after Wildey et al., 1966). Numbers with A and B indicate the direction of individual traverses.

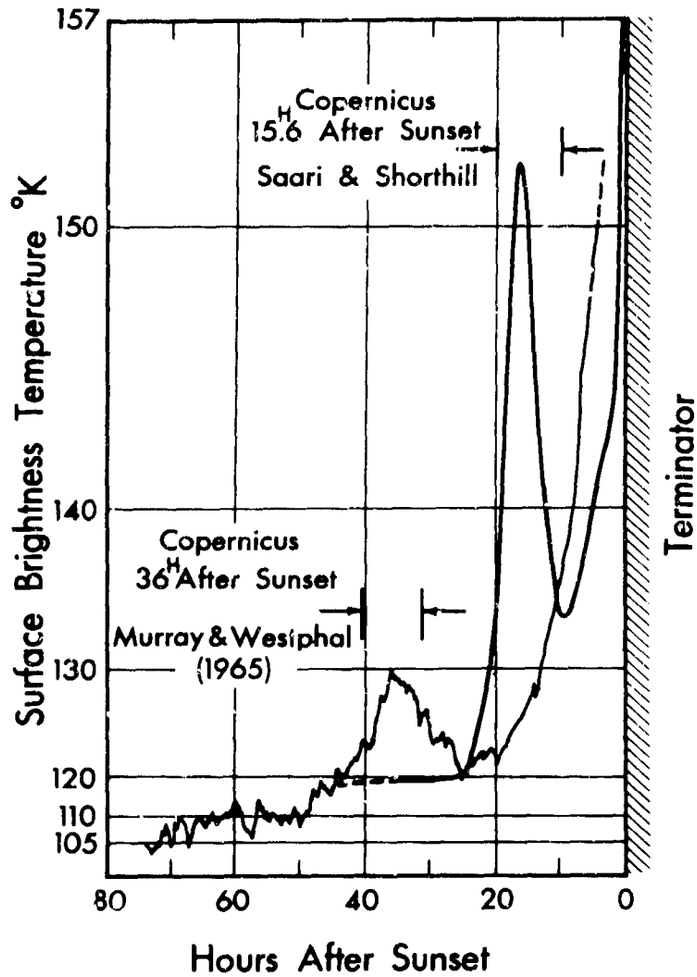

Fig. 13 Lunar nighttime traces through the crater Copernicus. The terminator temperature from the Saari and Shorthill data is 157°K while the data of Murray and Westphal (1965) indicate a value >150°K.

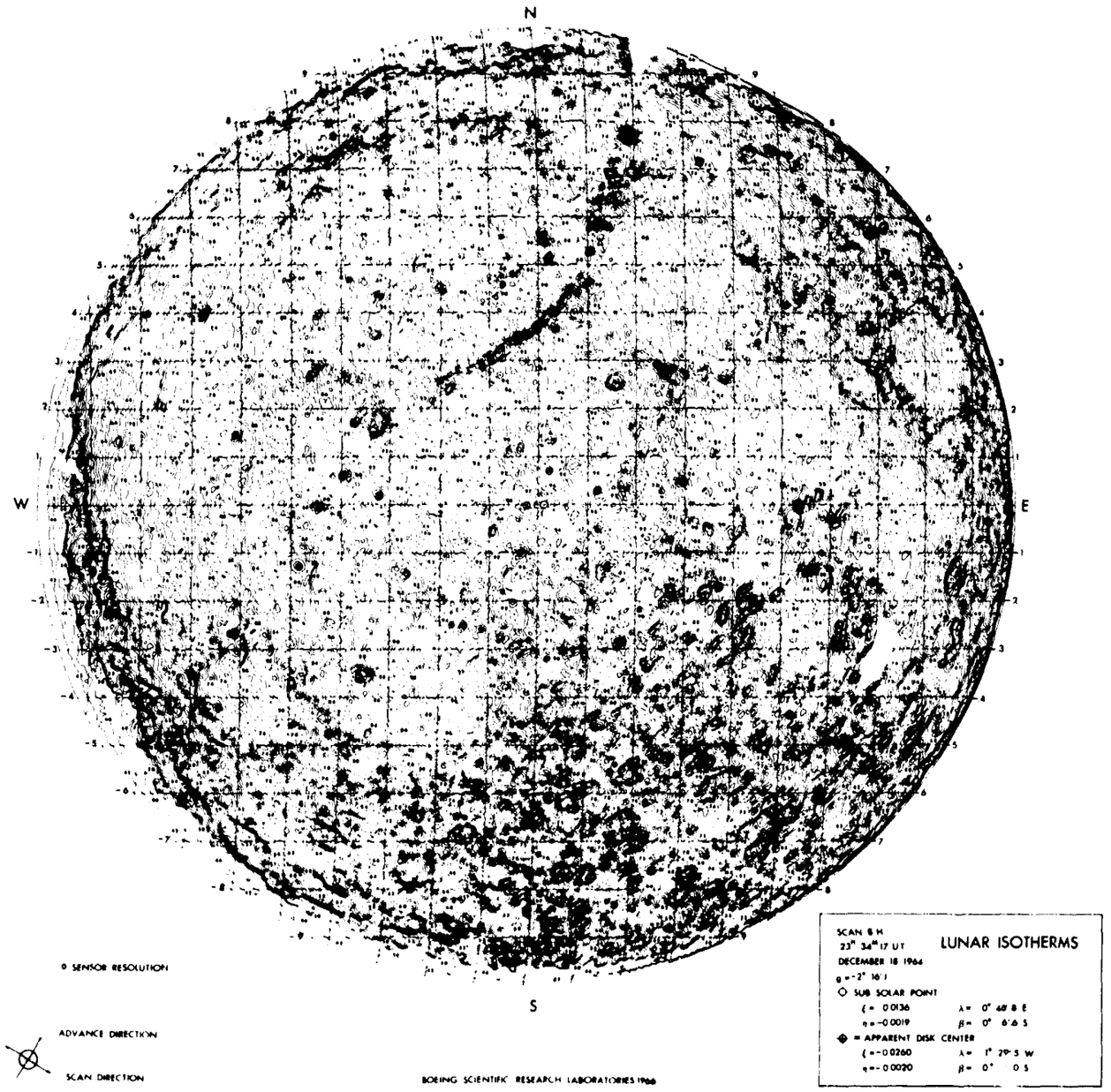

Fig. 14 Isothermal contours of brightness temperatures for the full moon. Temperatures may be determined by

$$T°K = 570.14/\log_{10}(2513.5/N - 1)$$

where N is the number printed on the con line.

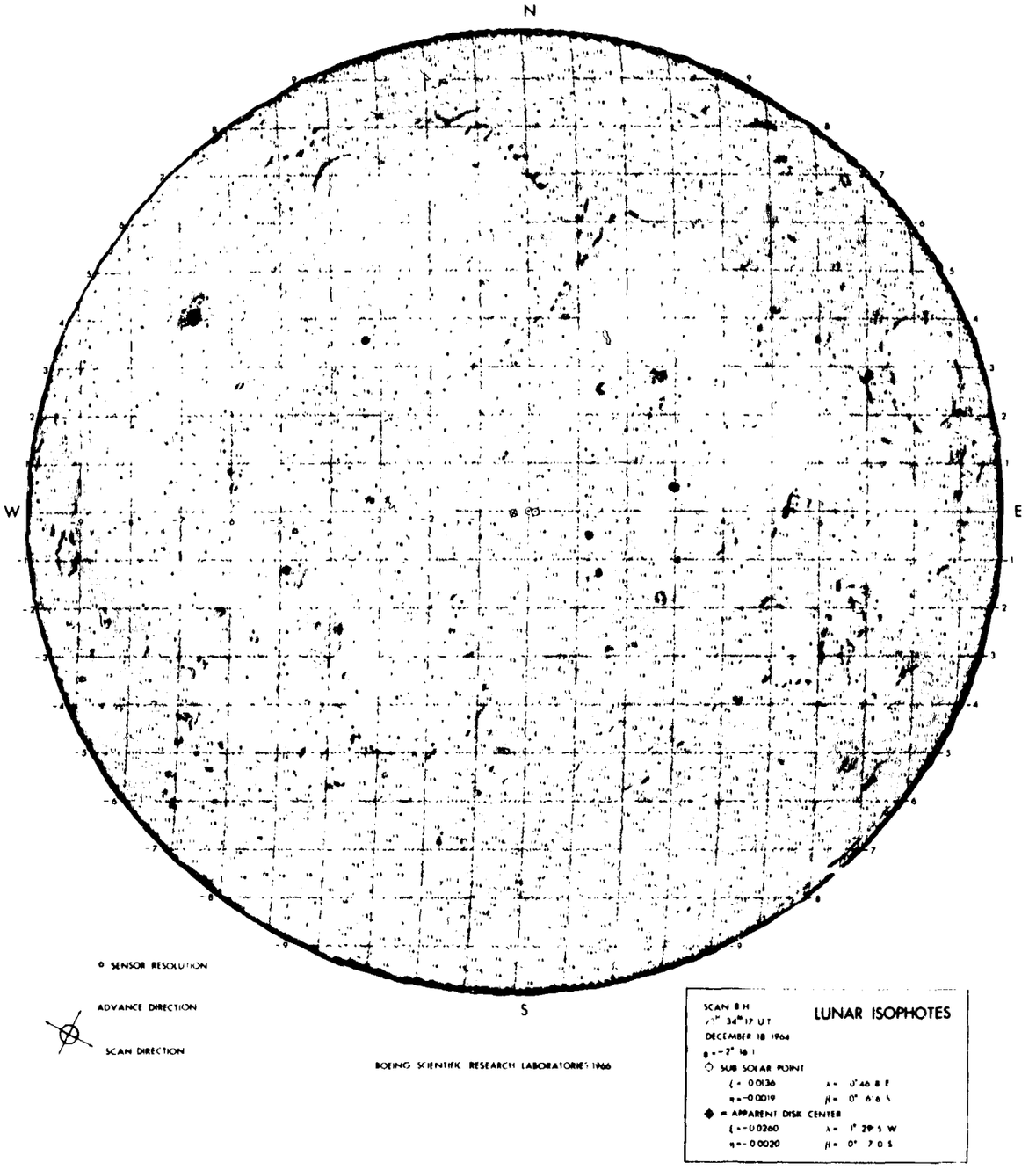

Fig. 15 Isophotic contours of rel ive brightness for the full moon. Albedo values according to Sytinskaya (1953) may be determined by A = 0.009064 C, where C is the number printed on the contour line.

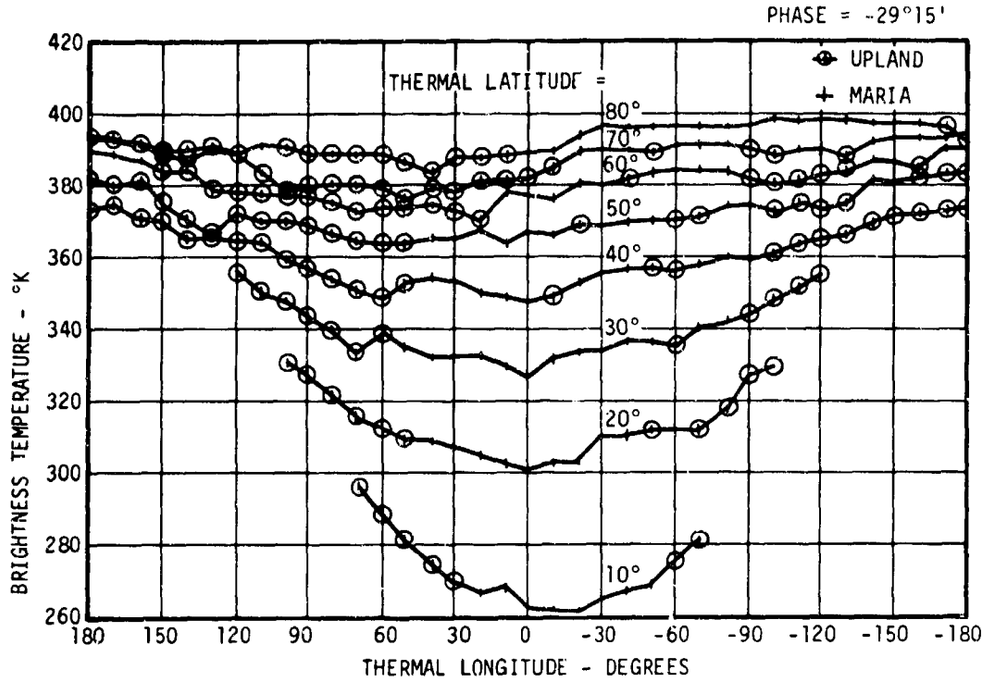

Fig. 16 Brightness temperature versus thermal longitude for phase angle -29°15'. The data are given for every 10° in thermal latitude (constant angular distance from the subsolar point).

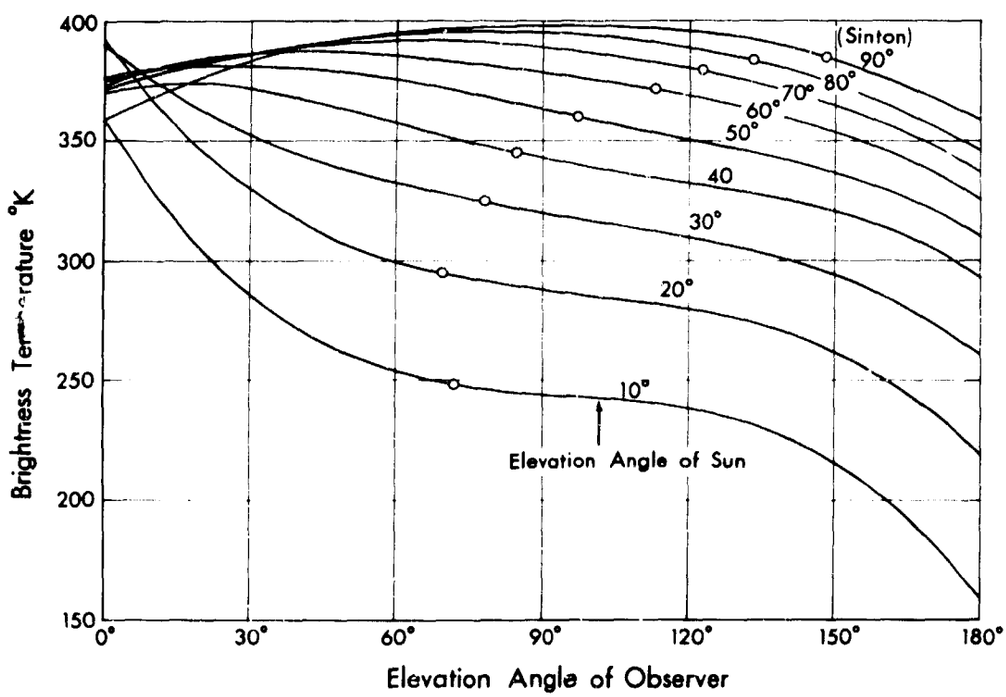

Fig. 17 Brightness temperature versus observer's elevation angle to the surface with the sun at different elevation angles. The data for 90° sun angle represents Sinton's observations of the subsolar point. The Lambert temperature is indicated by the open circles.

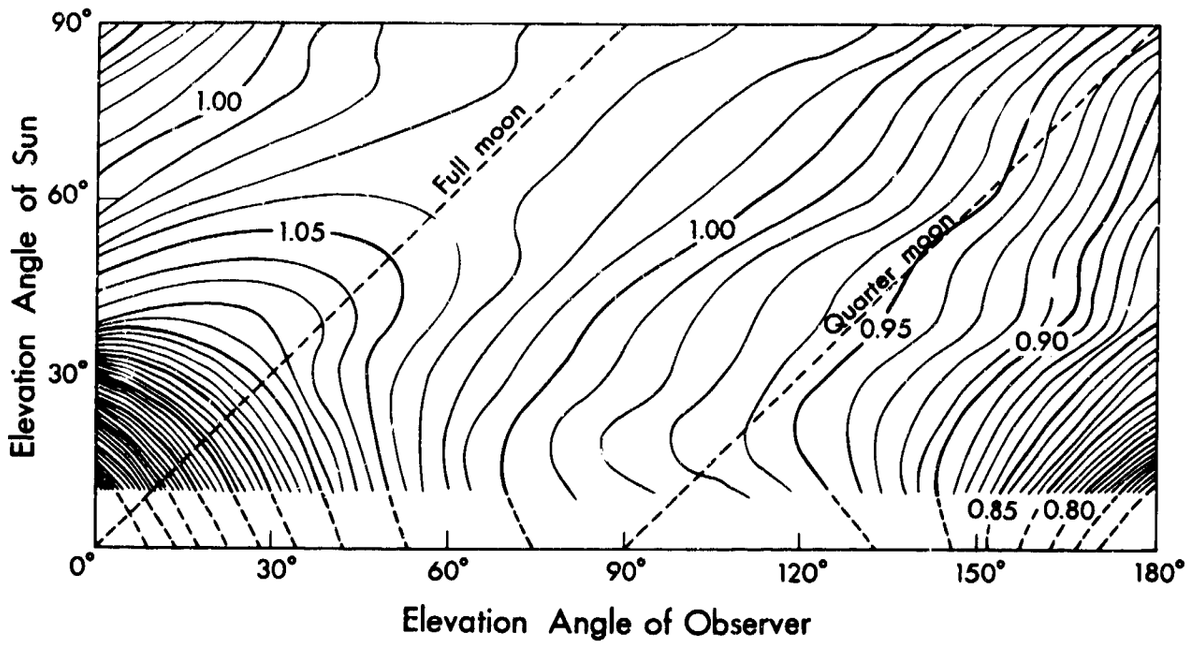

Fig. 18 Contours of the ratio of the brightness temperature on the thermal meridian to that of a Lambert surface as a function of the elevation angle of the sun and the angle of observation to the surface.

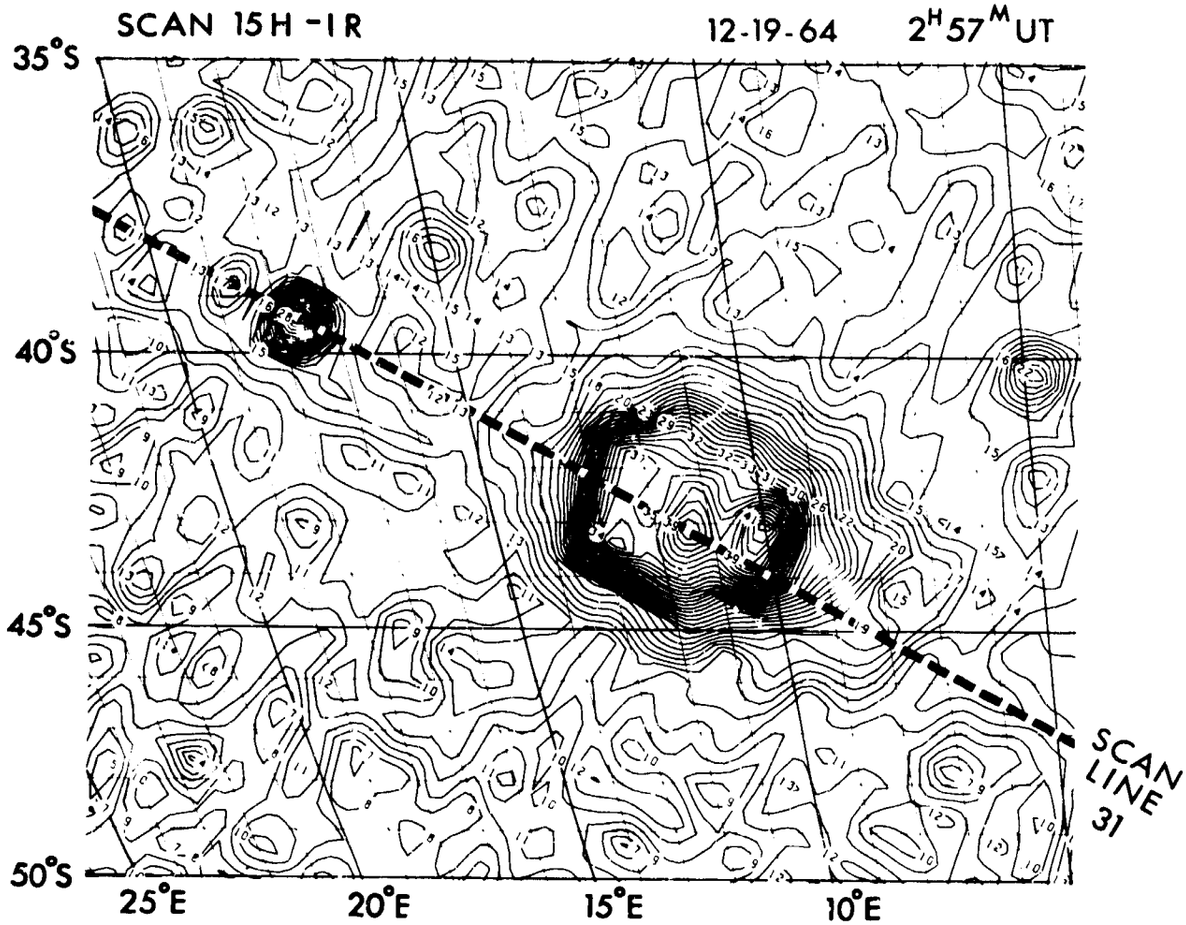

Fig. 19 Eclipse isothermal contours of brightness temperatures for the region of Tycho. Temperatures may be determined by $T°K = [redacted] + 2N$, where N is the number centered on the contour line. Note that man contours are not numbered.

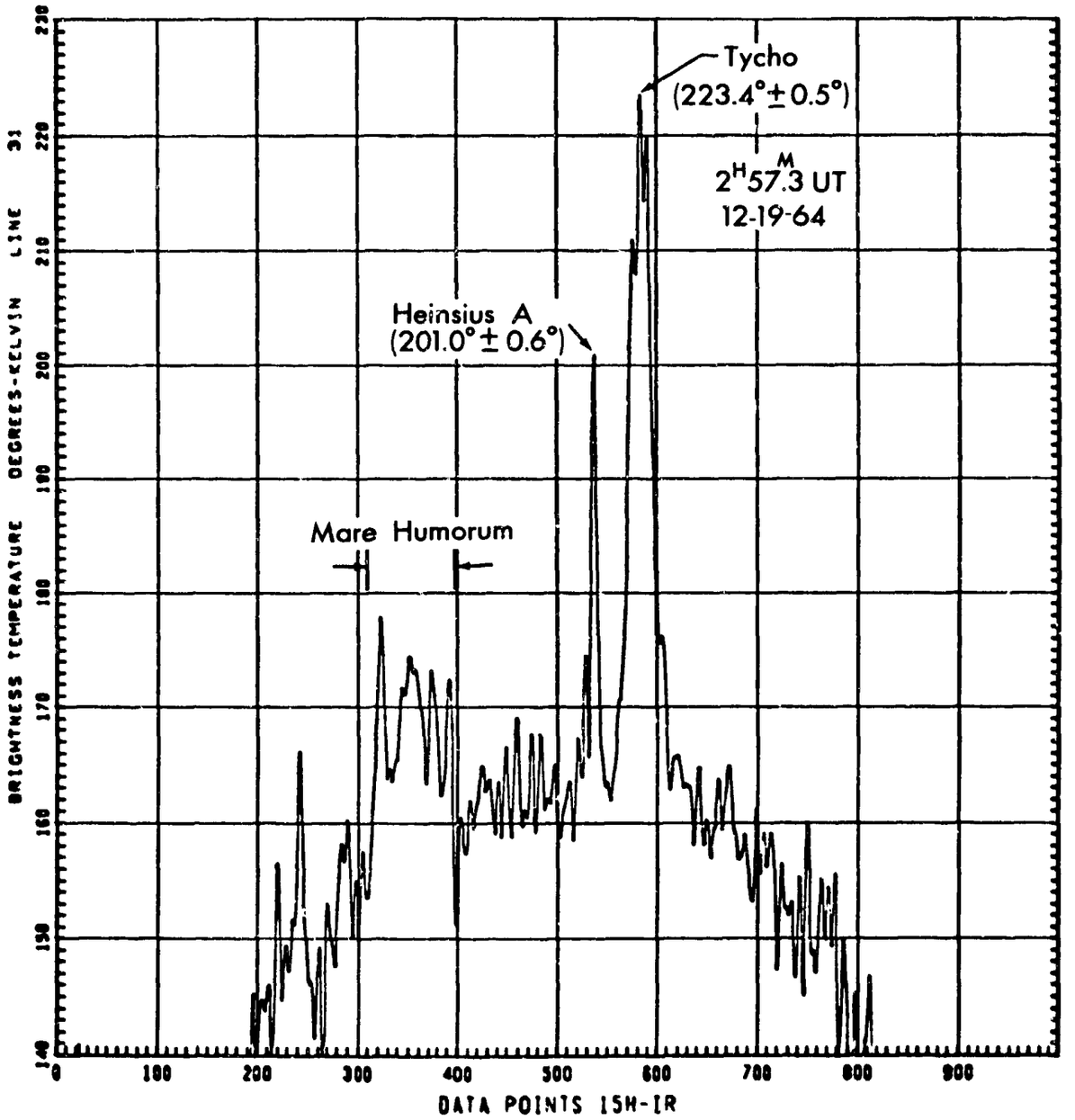

Fig. 20. Brightness temperature trace across Tycho during totality. A section of this scan line is shown in Fig. 19. The error in temperature was determined on the basis of the rms sky noise.

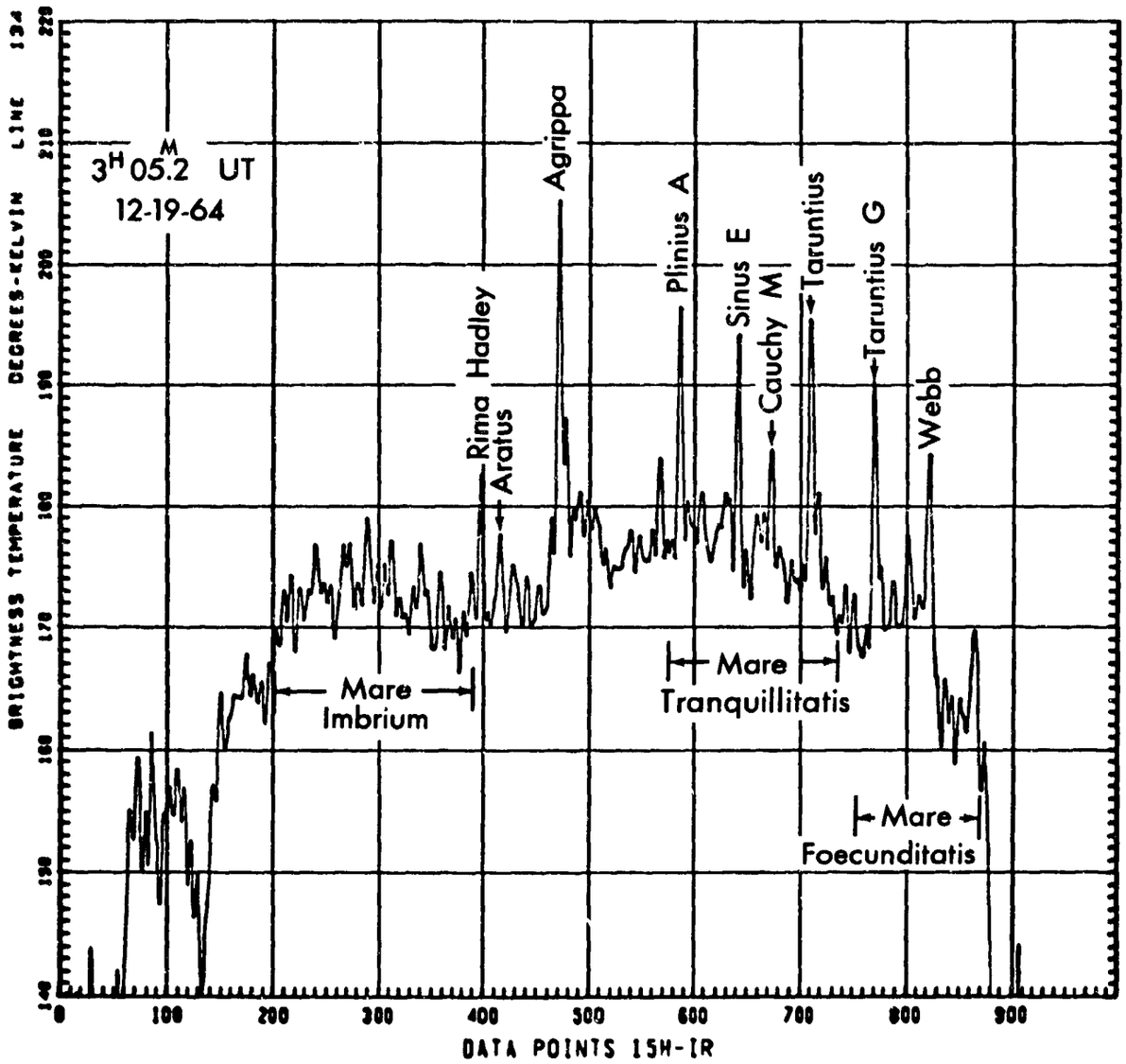

Fig. 21 Brightness temperature trace across the lunar disk north of the equator during totality. The general thermal enhancement of the maria can be seen.

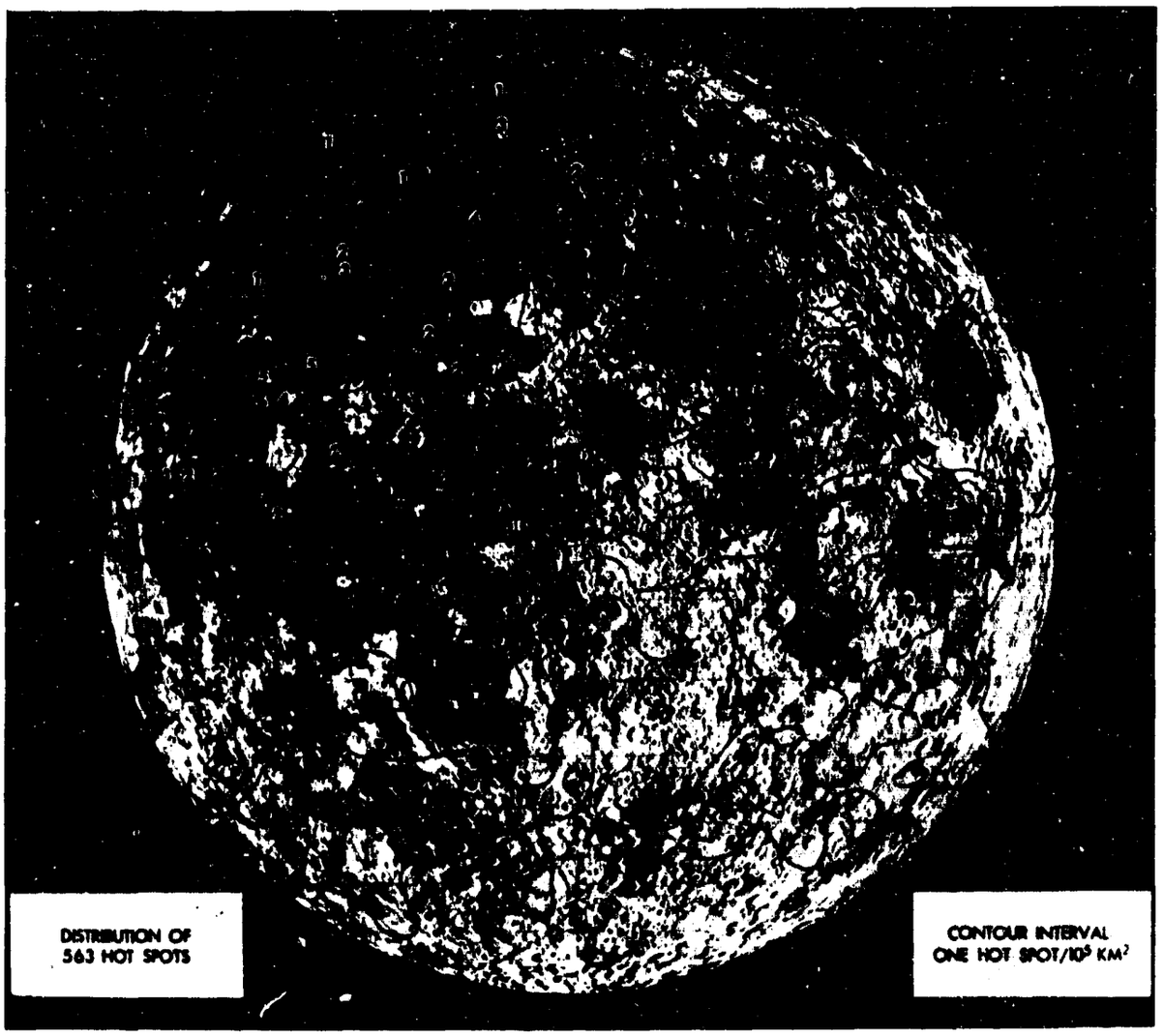

Fig. 22 Isodensity contours of the number of hot spots per 10^5 km^2 lunar surface.

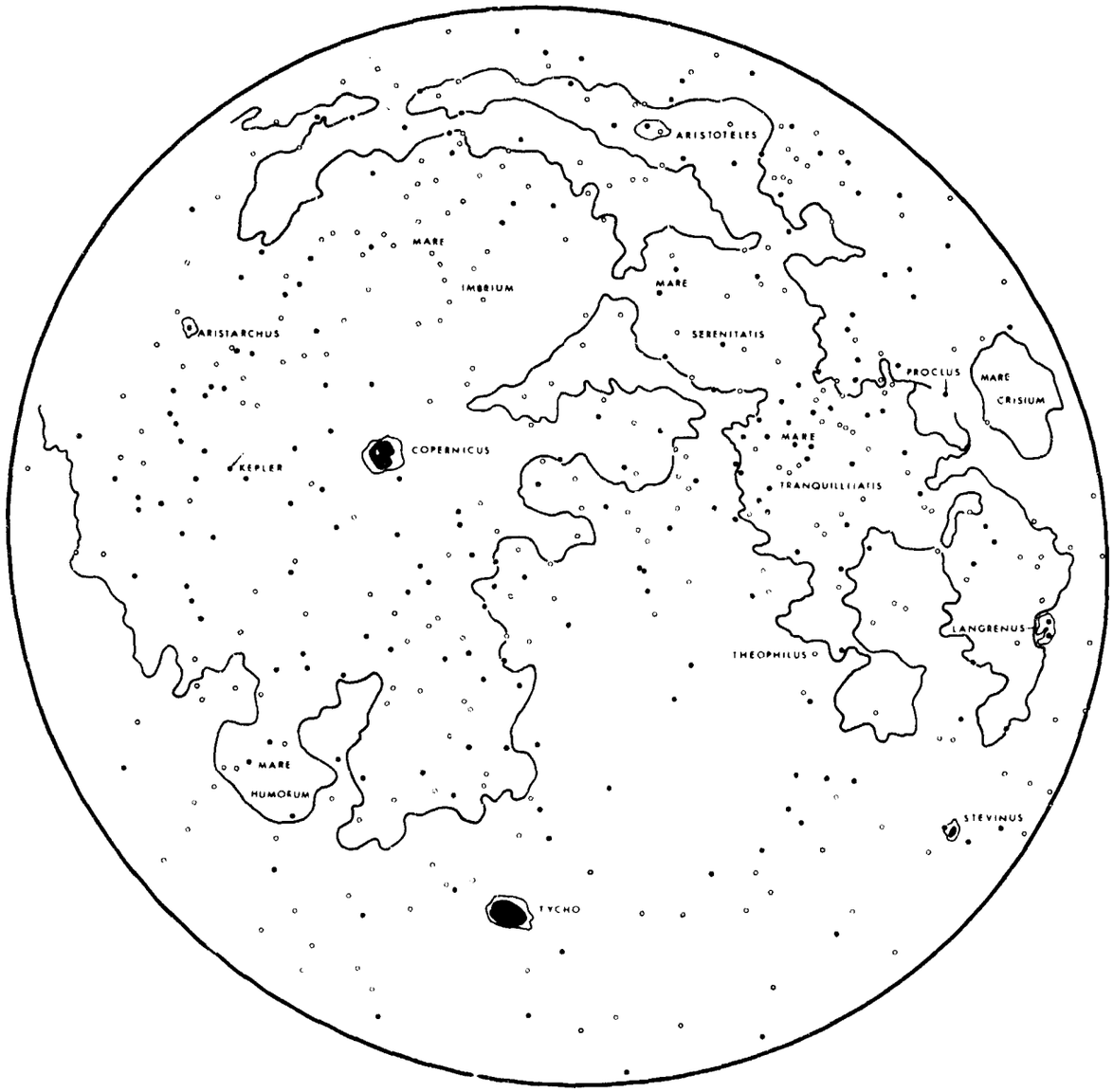

Fig. 23 Positions of 563 prominent hot spots on the lunar disk for the third scan in totality $3^H2^M.8$ UT, December 19, 1964. The solid circles represent the most prominent anomalies. The moon's outline appears out of round because of a slightly erroneous scale factor in one dimension during the mechanical process of combining scan lines.

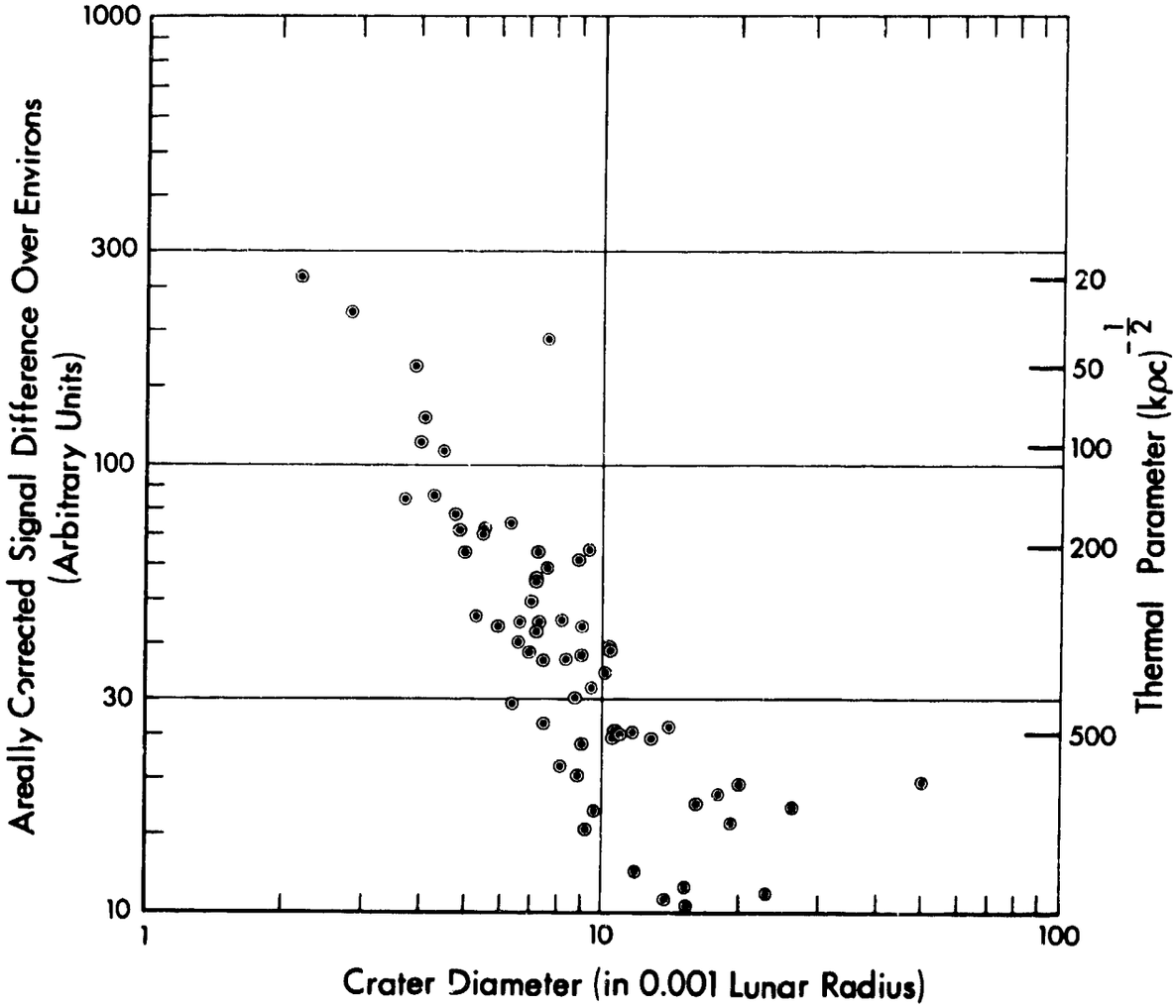

Fig. 24 Distribution of thermal anomalies versus crater diameters. Our resolution element corresponds to 0.01 of a lunar radius. The signal differences, when compared to the theoretical cooling of a homogeneous model of the lunar surface, correspond to the indicated values of the thermal parameter $\gamma = (k\rho c)^{-\frac{1}{2}}$, where k is the thermal conductivity, ρ the density, and c the heat capacity. This parameter has a value of about 20 for rock, 100 for dry sand, and 1000 for powdered dust in a vacuum (in calories and cgs units).

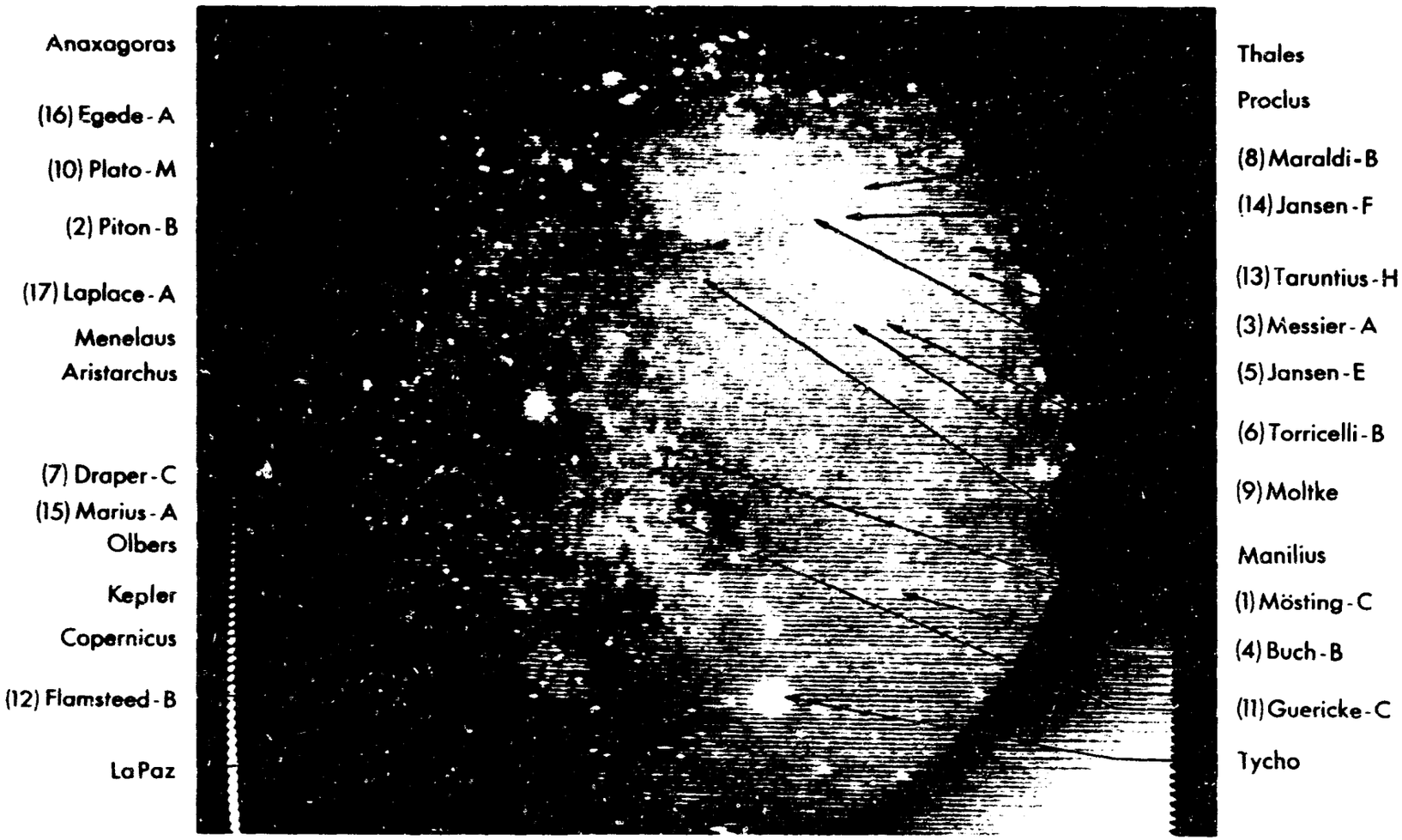

Fig. 25 Reconstructed infrared images of the totally eclipsed moon from 200 scan lines. The number indicates the ordering of hot spots to the areally corrected signal return given in Table 2. North is inclined 30° to the left of vertical.

Fig. 26 Lunar Atlas Chart overlaid with isothermal contours of brightness temperatures from the totally eclipsed moon. The dashed line shows the field of view from Lunar Orbiter II for the moderate resolution oblique photograph of Copernicus.

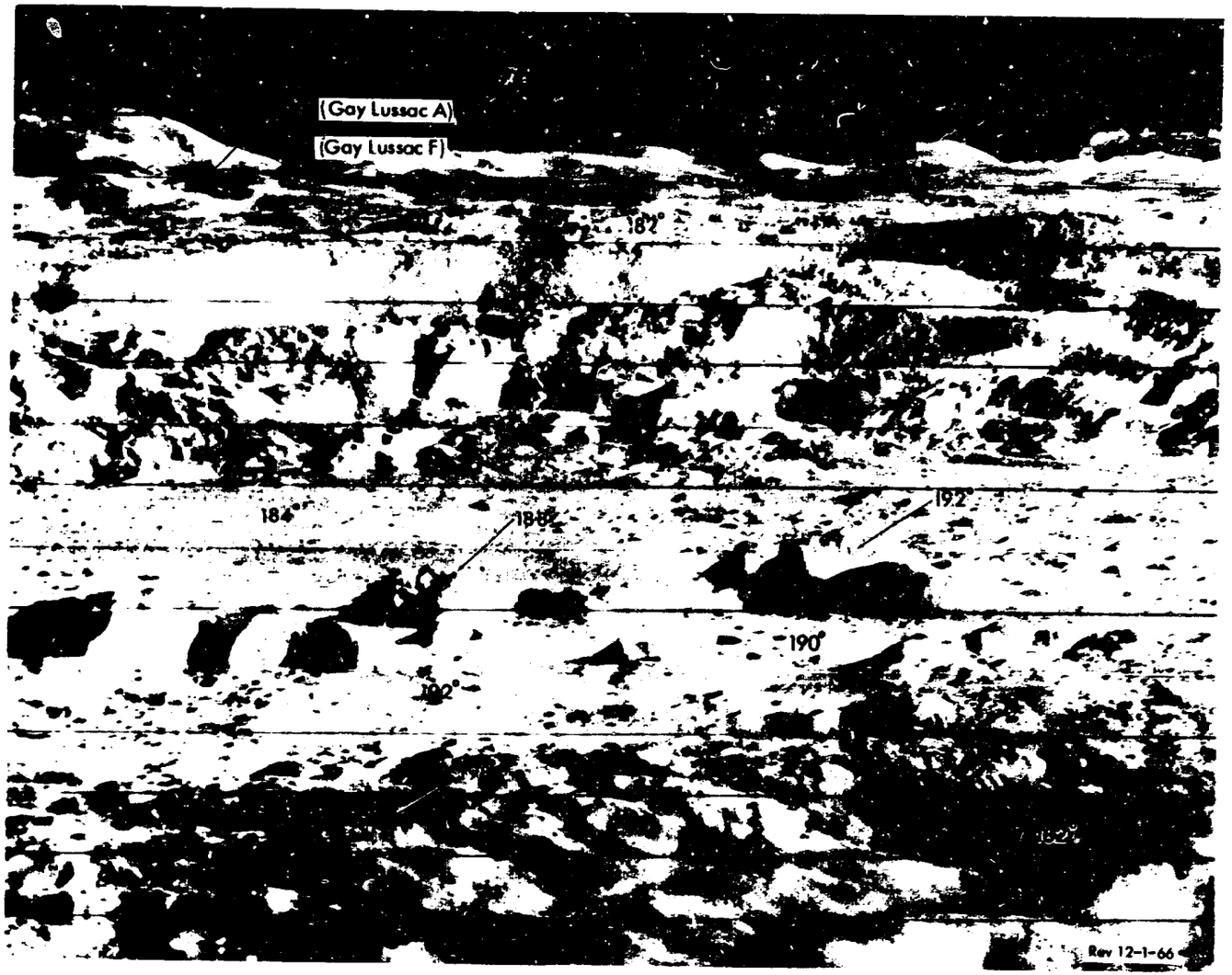

Fig. 27 The high resclution oblique photograph of Copernicus taken from Lunar Orbiter II. Eclipse brightness temperatures are indicated for certain extended regions (NASA photograph).

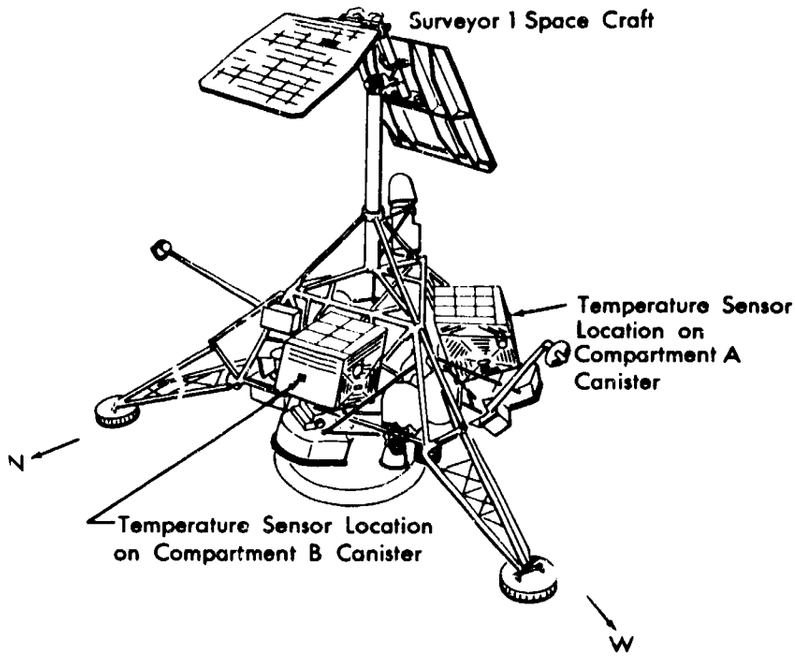

Fig. 28 Configuration of Surveyor I showing the position of the temperature sensor on Compartment A and B canisters.

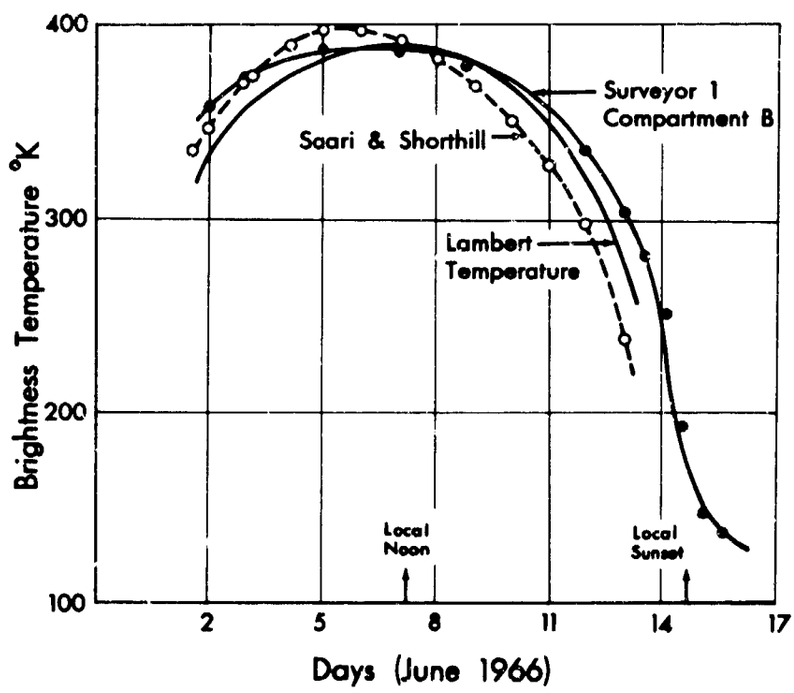

Fig. 29 Lunation temperature curves for the lunar surface at the Surveyor I site. The Lambert temperature is the solid line, open circles are earth-based measurements, and closed circles are the data obtained from the temperature sensor on Surveyor I Compartment B.

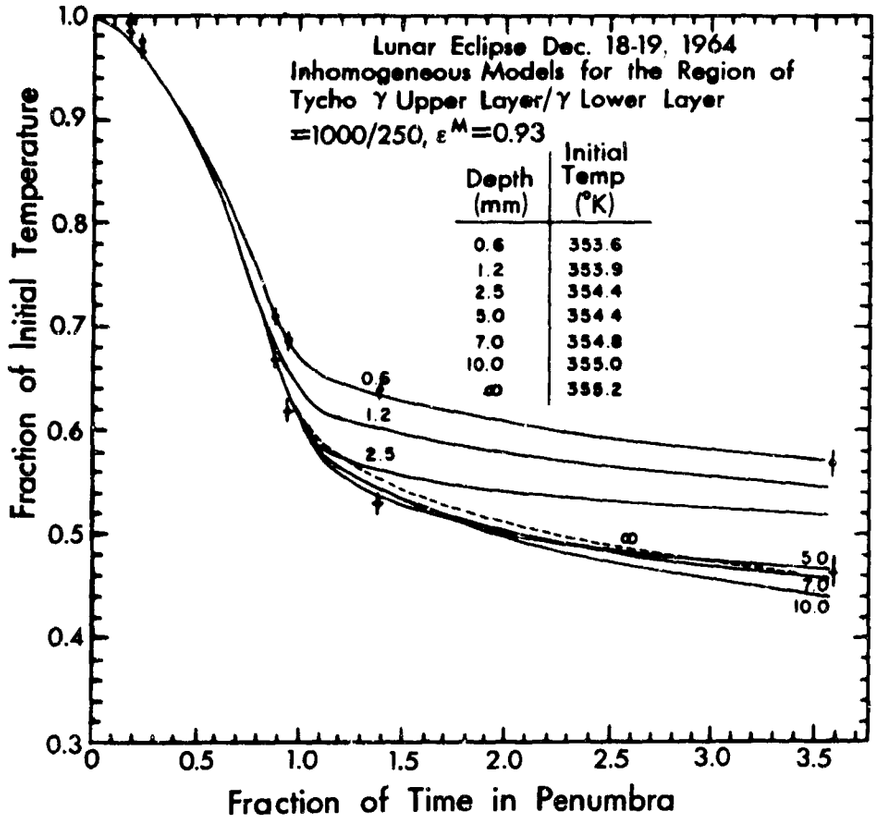

Fig. 30 Brightness temperature ratios for the crater Tycho (ϕ) and its environs (+). The family of theoretical curves was computed for two-layer models with temperature-independent thermal properties where γ is the thermal parameter $(k\rho c)^{-1/2}$, ε is the radiant emissivity and the upper depths are indicated (after Ingrao et al., 1966).

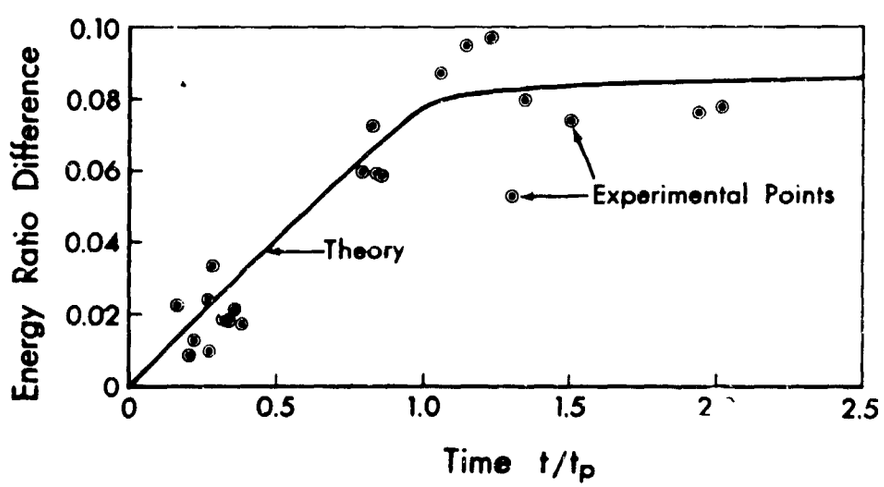

Fig. 31 Difference in energy ratios $(T/T_o)^4$ of the crater Aristarchus and interpolated environs during the eclipse of September 5, 1960. The abscissa is the ratio of time t to the duration of the penumbral phase t_p; T_o is the temperature at the onset of the eclipse (after Winter, 1966).

REFERENCES

Bastin, J. A., Lunar hot spots, *Nature 207*, 1381-1382, 1965.

Fudali, R. F., Implications of the nonuniform cooling behavior of the eclipsed moon, *Icarus 5*, 536-544, 1966.

Geoffrion, A. R., M. Korner, and W. M. Sinton, Isothermal contours of the moon, *Lowell Obs. Bull. 5*, 1-15, 1960.

Hapke, B. M., An improved theoretical lunar photometric function, *Astron. J. 71*(5), 333-339, 1966.

Ingrao, H. C., A. T. Young, and J. L. Linsky, A cri cal analysis of lunar temperature measurements in the infrared, i *The Nature of the Lunar Surface*, pp. 185-211, edited by W. N. Hess, D. H. Menzel, and J. A. O'Keefe, The Johns Hopkins Press, Baltimore, Maryland, 1966.

Jaffe, L. D., et al., Surveyor I Mission Report. Part II. Scientific Data and Results, *Technical Report No. 32-1023*, Jet Propulsion Laboratory, California Institute of Technology, 1966.

Low, F. J., Lunar nighttime temperatures measured at 20 microns, *Astrophys. J. 142*, 806-808, 1965.

Montgomery, C. G., J. M. Saari, R. W. Shorthill, and N. F. Six, Jr., Directional characteristics of lunar thermal radiation, *Boeing Document D1-81-0568; Brown Engineering Company Technical Note R-213*, 1966.

Murray, B. C., and J. A. Westphal, Infrared astronomy, *Sci. Am. 213*(2), 20-29, 1965.

Murray, B. C., and R. L. Wildey, Surface temperature variations during the lunar nighttime, *Astrophys. J. 139*(2), 734-750, 1964.

Pettit, E., Radiation measurements of the eclipsed moon, *Astrophys. J. 91*, 408-420, 1940.

Pettit, E., Planetary temperature measurements, in *Planets and Satellites*, edited by G. P. Kuiper and B. M. Middlehurst, pp. 400-428, University of Chicago Press, Chicago, Illinois, 1961.

Pettit, E., and S. B. Nicholson, Lunar radiation and temperatures, *Astrophys. J. 71*, 102-135, 1930.

Saari, J. M., The surface temperature of the antisolar point of the moon, *Icarus 3*, 161-163, 1964.

Saari, J. M., and R. W. Shorthill, Isotherms of crater regions on the illuminated and eclipsed moon, *Icarus 2*, 115-136, 1963.

Saari, J. M., and R. W. Shorthill, Thermal anomalies on the totally eclipsed moon of December 19, 1964, *Nature 205*(4975), 964-965, 1965.

Saari, J. M., and R. W. Shorthill, Isothermal and isophotic contours for the lunar disk through a lunation, *Boeing Document D1-82-0552-1*, 1966.

Saari, J. M., R. W. Shorthill, and T. K. Deaton, Infrared and visible images of the lunar surface during the eclipsed moon of December 19, 1964, *Boeing Document D1-82-0533* (same as AFCRL 65-886); also *Icarus 5*, 635-659, 1966.

Salisbury, J. W., and G. R. Hunt, Infrared images of Tycho on the dark moon, (to be published) 1966.

Sinton, W. M., A pyrometer for planetary temperature measurements, *Lowell Obs. Bull. 4*, 260-263, 1959.

Sinton, W. M., Eclipse temperatures of the lunar crater Tycho, *Lowell Obs. Bull. 5*, 25-26, 1960.

Shorthill, R. W., H. C. Borough, and J. M. Conley, Enhanced lunar thermal radiation during a lunar eclipse, *Publs, Astron. Soc. Pacific 72*, 481-485, 1960.

Shorthill, R. W., and J. M. Saari, Radiometric and photometric mapping of the moon through a lunation, *Ann. N.Y. Acad. Sci. 123*, Art. 2, 772-739, 1965*a*.

Shorthill, R. W., and J. M. Saari, Recent results of lunar eclipse measurements showing hot spots, in *Post Apollo Space Exploration*, Advances in the Astronautical Sciences, Vol. 20, Part 1, pp. 545-556, edited by F. Narin, American Astronautical Society, Washington, D. C., 1965*b*.

Shorthill, R. W., and J. M. Saari, Nonuniform cooling of the eclipsed moon: A listing of thirty anomalies, *Science 150*, 210-212, 1965*c*.

Sytinskaya, N. N., Catalog of the absolute values of visual reflectivity of 104 formations, *Astron. Zh. 30*, 295-301, 1953.

Wildey, R. L., B. C. Murray, and J. A. Westphal, (paper in preparation) 1966.*

Winter, D. F., Transient radiative heat exchange at the surface of the moon, *Boeing Document D1-82-0559*, 1966*a*.

Winter, D. F., Note on the nonuniform cooling behavior of the eclipsed moon, *Icarus 5*, 551-553, 1966*b*.

Zel'tser, M. S., The temperature of the lunar surface, in *The Moon: A Russian View*, edited by A. V. Markov, pp. 175-203, University of Chicago Press, Chicago, Illinois, 1962.

---

*We wish to thank the authors for making their data available prior to publication.